Technische Universität Wien

Fabrication of Nanoimprinted Polymer Surfaces for Immobilization and Signal Enhancement of Protein Arrays

MASTERARBEIT

zur Erlangung des akademischen Grades

Diplom-Ingenieur/in

im Rahmen des Studiums

Biomedical Engineering

ausgeführt von

Alma Salibasic

Matrikelnummer 0326655

Betreuer/in: Dr. Claudia Preininger (AITAustrian Institute of Technology)

Co-Betreuer: Univ.Doz.DI Dr.Georg Haberhauer (TU Wien)

Wien, 24. 11. 2012 _____

Abstract

Protein arrays are attractive analytical devices in medical diagnostics as they allow detecting multiple parameters in parallel. In order to meet clinical requirements, significant improvements need to be made. Especially in this context, development of biosensors using polymeric nanostructures is a promising approach since nanostructures increase the surface area and thereby improve protein immobilization and assay performance. Although a large number of works on nanostructured protein arrays have been reported, the impact of polymeric nanostructures on signal enhancement and protein array performance has not been fully addressed yet.

Primarely, nanoimprint lithography (NIL) as a high-throughput, low-cost, nonconventional method has been employed and studied for fabrication of diverse polymeric nanostructures. Stamps made of sPDMS, hybrid PDMS and Ormostamp material were produced from various masters. The stamps with a replicated surface relief were then imprinted into resist materials such as mr-IT85 and EPON 1002F typically used for thermal nanoimprinting (T-NIL) and UV-curable resist Amonil MMS 10 used for UV nanoimprinting. Surface characterization of imprinted substrates was performed using atomic force microscopy (AFM), contact angle analyzer and autofluorescence scanning. Further, several additional experiments were conducted to study stamp durability and reproducibility.

Furthermore, EPON 1002F and Amonil chips were incubated with CRP antigen and analytes binding was then detected using Dy647-anti CRP and Dy547-anti CRP. Best chip performance was achieved on EPON 1002F imprinted with sub 120 nm grating structures.

Acknowledgments

During these intense eight months I've been working under the patient and encouraging supervision of Dr. Claudia Preininger and Mag. Ursula Sauer.

The work presented in this thesis has been carried out at AIT Austrian Institute of Technology with the support and great working atmosphere of all the colleagues and friends at the AIT Biosensor group. Lastly, I thank my graduate Professor Georg Haberhauer for his continuous support.

Table of Content

Motivation

Protein microarrays are attractive high throughput analysis tools to study fundamental aspects of cellular protein expression and protein function and are typically used for drug screening, biomarker discovery, clinical immunological assays, biosensors and more[1-5].

The successful development of protein arrays for biomedical applications heavily depends on the understanding and control of the protein-surface interaction. Especially in this context, development of biosensors using polymeric nanostructured platforms is a promising approach since nanostructures increase the surface area available for protein immobilization and thus have direct impact on signal strength.

In order to substantially improve the understanding of the protein-surface interactions and to realistically pave the way to an effective nanostructured surfaces rational design, it is fundamental to characterize, to understand and to control the material surface design parameters (chemistry, topography) and the basic biological mechanisms that determine protein behavior on artificial substrates [6].

In this thesis we address these issues. In the first part, we employ nano-imprint lithography, a high throughput, and low cost patterning method that is able to create nanostructured surfaces. We investigate several organic-inorganic photoresist materials and dedicate special attention to spin coating of thin films as one of the most important requirements to the high throughput fabrication of biocompatible substrates with controlled nanostructure. We further use three commercially available stamp/mold materials with different moduli and study stamps durability, reproducibility and transfer accuracy. In the second part, we employ nanostructured surfaces for protein immobilization and investigate the effect of differently patterned surfaces on signal enhancement and protein assay performance.

1 Introduction

This work deals with the fabrication of polymeric nanostructures, and their implementation in microarrays to serve as platform for protein immobilization and a strategy for signal enhancement. In this chapter, we present an overview of the employed methods and techniques:

In the section 1.1, a brief introduction in Nanoimprint Lithography (NIL) is given, followed by a discussion about the two most important types of NIL processes i.g. thermal nanoimprinting lithography (T-NIL) and UV-based nanoimprint lithography (UV-NIL). The masters are defined in section 1.2, followed by a discussion of the material aspects of stamps in 1.3, anti-sticking layer in 1.4 and resist materials in 1.5. The basics of the film deposition process will be discussed in section 1.6. Surface characterization of the nanostructured arrays is discussed in section 1.7. In the last section i.g. 1.8, a brief overview of protein microarrays is given, followed by a detailed explanation of immunoassay formats, protein immobilization approaches and detection methods.

1.1 Nanoimprint Lithography

The drive to miniaturize devices and increase storage densities has pushed research on nanotechnology, including methods to construct polymeric nanostructures, which are important in the development of sensors, biotechnology, catalysis, and electronic and optical devices at a nanometer scale[7].

Many methods have been developed to fabricate micro- to nanostructures of polymers. Photolithography is typically utilized in the semiconductor industry due to its high throughput [7]. However, photolithography is limited in resolution by the wavelength of light. Direct write electron and ion beam lithography have demonstrated sub 10 nm [8]. However as the features' size scale down, new challenges are emerging to drive the cost up dramatically [9]. In that context, nanoimprint lithography (NIL) introduced by Chou et al. [10] has shown promise as new disruptive technique to replace photolithography and electron beam lithography (EBL) in patterning electronic and optical devices due to its throughput with easy operation at low cost [9]. Based on mechanical deformation of a resist, nanoimprint

lithography is a high-throughput technique able to achieve pattern resolutions beyond the limitations set by the light diffraction of projection lithography techniques [10]. Unlike conventional lithography methods, imprint lithography itself does not use any energetic beams [11]. It also does not require extreme ultraviolet light sources and special optics, which increase the cost dramatically[11]. Therefore, nanoimprint lithography's resolution is not limited by the effects of wave diffraction, scattering and interference in a resist, and backscattering from a substrate[12].

Being a next generation lithography candidate, NIL does not have any limitations in pattern geometry [13]. Moreover, NIL is conceptually very simple, provides parallel processing with high throughput, extremely good resolution and a relatively fast replication process [13].

There are two types of NIL, e.g. thermal nanoimprinting lithography (T-NIL) based on hot embossing of thermoplastic polymers and UV-based nanoimprint lithography (UV-NIL) based on UV-curable polymers.

1.1.1 Thermal Nanoimprint Lithography

Thermal-NIL is the earliest and most mature nanoimprint lithography developed by Chou et al. [10] in 1995. The thermal nanoimprint process, as illustrated in *Fig. 1* can be described in four steps: (*Fig.1-1*) a thermoplastic resist is spin coated on the substrate; (*Fig.1-2*) after prebake, the thermoplastic resist is heated above the glass transition temperature and the stamp with the predefined topographic patterns is brought into contact with the polymer; (*Fig.1-3*) once the polymer has filled all the cavities of the stamp, the substrate and the stamp are cooled down to below resist glass transition temperature and the stamp is separated from the substrate in a so called de-molding step, leaving the negative replica on the substrate; (*Fig.1-4*) the patterns are transferred into the resist to the underneath substrate [12]. The subsequent pattern transfer is usually achieved by anisotropic etching, such as reactive ion etching (RIE) and includes removal of the undesired residual layer that is formed during the imprint process.

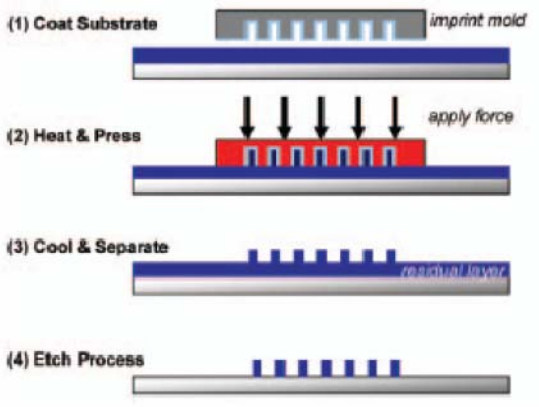

Fig.1: The process flow of thermal NIL [14].A thermoplastic resist is spin coated on the substrate (1), the thermoplastic resist is heated above the glass transition temperature and the stamp is brought into contact with the polymer (2), the mold is separated from the sample and the pattern resist is left on the substrate (3),etching is applied to transfer the pattern in the resist to the underneath substrate (4).

1.1.2 UV- NIL

The NIL-process using UV-curable polymers is called UV-NIL. In the UV-NIL process, the pattern transfer occurs, similarly to the T-NIL process, by mechanical deformation of the resist material. A four step UV NIL process is shown in Figure 2. First, a layer of UV- curable resist is spin coated on the substrate (*Fig. 2 -1*). Then, the transparent stamp is brought into contact with the resist, low viscosity UV curable resist material flows into the cavities of the stamp and is cross-linked into the rigid pattern upon exposure to UV light (*Fig.2-2*). In this case, the stamp needs to be not only mechanically robust, but also UV transparent [15]. Subsequently the stamp is released from the imprinted substrate (*Fig.2-3*), pattern is transferred into the substrate (*Fig.2-4*).

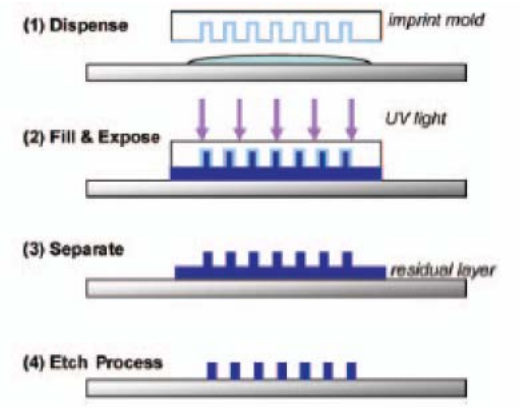

Fig. 2: Schematics of UV-NIL [14]. UV curable resist is spin coated on the substrate (1). Substrate stamp assembly is exposed to UV light to harden the resist at room temperature (2). The stamp is separated from the substrate (3). Residual layer is removed by an anisotropic plasma etch process if necessary (4).

1.1.3 Comparison between thermal and UV NIL

Compared with each other, both of those two NIL approaches have their prominent advantages. In the UV NIL process, the transfer is carried out at room temperature and at low pressures thus avoids time consuming heating and cooling cycle's process for T-NIL. Furthermore, due to the lower viscosity of the UV curable photoresists, the cavity filling can occur easier than in the T-NIL process [16-17]. The major differences of the process variations of NIL are summarized in *Table1*.

Table 1: Comparison of T-NIL and UV-NIL [18].

Type of NIL	T-NIL	UV-NIL
Resist	solid thermoplastic Tg ≈ 60-100 C	liquid, UV curable
Viscosity	10^{3}-10^{7} Pas	10^{-2}-10^{-3}Pas
Pressure p	20-100 bar	0-5 bar
Temperature T (imprint)	100-200 °C	Room temperature
Temperature T (demold)	20-80 °C	Room temperature (ambient)
Imprinting Time	from seconds to minutes	< 1 min (per exposure)
Advantage	low-cost, large-area, wide choice of template material	low viscosity, low pressure, ambient temperature
Limitation	high temperature, high pressure and long process time due to repeated heating and cooling processes	step and repeat needed for large areas, low viscosity materials are too volatile to form stable films.

1.2 Master

Masters are templates made of rigid materials such as silicon or siliconoxide and carrying three dimensional patterns on their surface. These masters are typically fabricated using time-consuming and expensive techniques such as photolithography for patterns in the µm range, e-beam lithography for sub µm patterns, and focused ion beam for fabrication of large and complex nanopatterns.

1.3 Stamps/Molds

The stamps or molds are a fundamental and central element in the imprinting process because they contain the imprint patterns which directly determine the nanoimprint resolution [19]. The working stamp is made out of polymeric materials and represents the initial replica of the master thus carries the opposite pattern of their surface. Fabricating various working stamps from a single master and using these stamps instead of the expensive master for NIL process, can prevent damages to the expensive master structure. This makes the use of a flexible stamp very attractive from an economical point of view.

Great care must be taken in considering a proper material for NIL stamp creation since the chosen material directly affects the stamp lifetime and reliability [16]. Various processes that can be used for replication in NIL allow one to choose from a wide selection of stamp materials, ranging from soft organic or polymeric materials such as PDMS, Teflon, polyurethane or perfluoropolyether (PFPE) or hard materials like quartz, Ni, Si, and SiO_2[15].Hard materials offer better structural integrity due to high stiffness, while soft materials might undergo structural degradations over time to some extent, but provide relatively simple stamp fabrication[16].

An ideal stamp material provides necessary hardness for the stamp, is thermally stabil and/or UV transparent, provides low pattern dimension irregularities under the imprinting conditions, reliable releasing properties during the demolding process [20], and does not undergo chemical reactions with the imprinting material. Also issues related to processability, transparency, conductivity, availability, cost and easy handling are of great importance[21].

The most commonly used material in fabricating of soft stamps for NIL applications is poly (dimethylsiloxane) PDMS. This thermocurable siloxane organic polymer, which meets many of the requirements listed above, is characterized by a highly open, flexible and mobile Si-O-Si backbone [20] which enables replication of relief shapes. LowYoung's modulus, as another attractive property of PDMS, enables conformal contact with the surface without applying pressure. Furthermore, PDMS offers a high elongation at break (> 150 %) [22],and its copolymer film forms a lower surface energy component allowing easy mold-resist

detachment, whereas at the same time form higher surface energy component and thereby provides good adhesion to the substrate[20].The PDMS high UV transparency allows its use as a mold for UV curable materials in the UV-NIL process (wavelengths from 350 to 450 nm [17, 23]).In addition, PDMSis easy to mold and to clean, commercially available at low cost and non-toxic. However, despite its high popularity, using PDMS as stamp material has some drawbacks such as mechanical weakness, intolerance for organic solvent during the interaction with the resist [24, 25]. Although, lowYoung's modulus as mentioned before allows conformal contact with the surface, relatively low modulus of PDMS can lead to structural problems in the pattern transfer elements, especially for nanometer features [26]. Typical deformations related to the low compression modulus (2.0 Nmm^{-2}) of Sylgard 184 PDMS cause the stamp to deform, patterns roof to collapse or sag. Also rounding of the relief features by surface tension between stamp and master as well as lateral collapse or pairing of replicated features may occure[27].

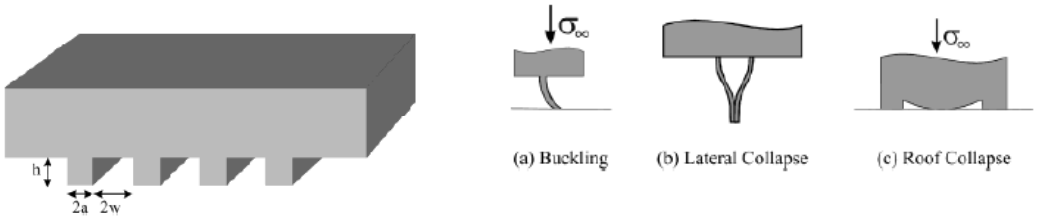

Fig.3: **Typical stamp deformations during NIL process:(a) buckling, (b) lateral collapse, and (c) roof collapse [29].**

Roof collapse is strongly related to pattern topography. Stamps with wide and shallow relief features tend to collapse or buckle under their own weight in contact with the surface. On the other hand, low aspect ratio features are unable to withstand compressive forces and adhesion between the stamp and substrate and hence tend to sag[28].*Latteral collapse* occurs when the closely spaced features adhere to each other laterally due to high capillary forces. [30,31]. In addition, during cure molding process, PDMS high expansion coefficient (260 $\mu mm^{-1} C^{-1}$) can also lead to structural deformations and its surface energy is not low enough (25 $nM m^{-1}$) for high fidelity transfer [32].

To overcome these problems and improve the resolution and generation of patterns with high fidelity, careful modification of the conventionally used PDMS material and the stamping technique is required. Schmid et al[29] developed a stiffer stamp material, a

polymeric composite, based on vinyl and hydrosilane end-linking polymers, so called hard PDMS (hPDMS) which has higher compression modulus (9 N mm^{-2}) [33,31]. The hPDMS uses shorter cross-linkers [33,31]compared to those in the 184-PDMS[27], but its elongation at break is much lower than that of 184-PDMS [33, 27]. To make the stamp less brittle, *Odom et al* [27] fabricate a composite stamp that consists of a thin layer of h-PDMS and a thick backing layer of Sylgard 184 material.

Another recently developed stamp material for transparent stamp fabrication in imprint lithography was developed by micro resist technology GmbH and commercialized under the name Ormostamp. The Ormostamp is a UV curable inorganic-organic hybrid material, significantly harder than *h*PDMS. The fabrication of Ormostamp stamps is fast, easy and cost-efficient, because only small material amounts are consumed within the process. Moreover, high transparency and high thermal and chemical stability (stable up to 270 °C, resistant to commonly used solvents and NIL materials) enable a successful application especially in UV-based nanoimprint lithography [32].

1.4 Release agent (Anti-sticking layer)

One of the key issues for successful NIL especially when working with hard stamps is to control the defect of the stamp. With down-scaling the nanometer- sized features on the stamp, the increased contact area between the interface of the mold and the substrate makes the de-molding step during stamp fabrication and imprinting process critical [34]. Hence, the anti-adhesion properties on the stamp become more pronounced [35]. Anti-adhesion layers are used to reduce the possible interaction between mold and resist by minimizing the surface energy of the mold. A low surface energy release layer on the stamps helps to reduce friction of the patterned features. It also increases the stamp´s lifetime by preventing surface contamination but has to be thin and durable [20].

When working with nanostructured surfaces, the chosen deposition method of the anti-adhesion layer is highly important. Liquid phase deposition methods are disadvantageous due to insufficient wetting of the hydrophilic stamp material by the hydrophobic solvent. On the contrary, vapor phase deposition is advantageous due to the covalent linking of an anti-adhesion monolayer over a large area [35]. Among many others, Tridecafluoro-(1,1,2,2)-

tetrahydrooctyl- trichlorosilane (F13-TCS) presented by Beck et al [34] is a very attractive anti-sticking coating due to its easy implementation and good durability.

1.5 NIL Resists

Another important component of NIL is the imprinting resist. Since the NIL process is based on mechanical deformation of the resist by the stamp, selection of the material for use as NIL resist shall consider their critical properties such as aspects of correct pattern replication, modest imprint temperature and pressure, etch selectivity and proper mold – resist release during de-molding step. [21].

An ideal resist for NIL applications possesses high surface energy ensuring strong adhesion to the substrate, lower Young's modulus compared to that of the mold, good release properties during the de-molding process while not compromising the adhesion of the mold to the substrate [36, 37].To complete the imprinting process within a practical time frame, the resist material shall also have a sufficiently low viscosity [38,36].

Dependent on the process type, materials used in NIL can be categorized into two main types: thermoplastic materials mostly used in T-NIL, and thermosetting or curable materials used in UV-NIL.

1.5.1 T-NIL resist materials

These materials offer the possibility of controlling the viscosity by temperature. In thermal NIL, the temperature is risen above the glass transition temperature (T_g) ca. 70 –90°C so that a polymer material reaches viscous flow state and fills the cavities. In the demolding step, the temperature is decreased to below T_g of the polymer to ensure the imprinted patterns after the mold is removed[36].Choosing the proper imprinting temperature is of great importance in terms of achieving high-quality imprints. The imprint temperature must be high enough to partially cross-link the pattern. If the temperature is too high, the material will cross-link too much before the imprinting process is completed, inhibiting the flow of material into the stamp cavities [17].

Another critical property of thermoplastic resists is the molecular weight M_w. The polymer molecular weight defines many physical properties such as temperature for transitions from

liquid over viscoelastic to solid, and mechanical properties such as stiffness, strength, viscoelasticity, toughness and viscosity. If the molecular weight M_w is too low, the transition temperature will be low as well[20]. While high molecular weight polymers such as poly(methyl methacrylate) PMMA are normaly used in e-beam lithography (EBL), polymers with low molecular weight of some tens of kg/mol are patterned in NIL due to mobility of short chains to move more easily into small mold cavities[20]. In practice, low-molecular weight polymers can be imprinted at lower temperatures, lower pressures, and within shorter times. For these reasons, the choice of both T_g and *M*w is important in maintaining the structural stability of the imprinted patterns [36].Manyinstitutes have developed thermoplastic resist materials and optimized them to be used for various NIL processes types and tools e.g. Nanonex (e.g. NXR 1000), micro resist technology (e.g. mr-IT85 and mr-NIL 6000).

1.5.2 UV curable resists for UV-NIL

UV curable resist materialshave to possess specific characteristics such as low viscosity,high curing speed, high etch-resistance, high adherence to the substrate, low adherence to the mold, reduced contraction during photopolymerization, adapted mechanical properties and finally a low evaporation rate. To meet the various processing demands of UV-NIL, the imprint material is typically comprised of a monomer portion and at least one cationically polymerizable functional group, a crosslinker reactive with the first component, and a cationic photoinitiator. Upon exposure to UV light, the material composition crosslinks to form a cured resist film that is the reaction product of the first component, the crosslinker, and the cationic photoinitiator as shown in *Fig. 4*[39].

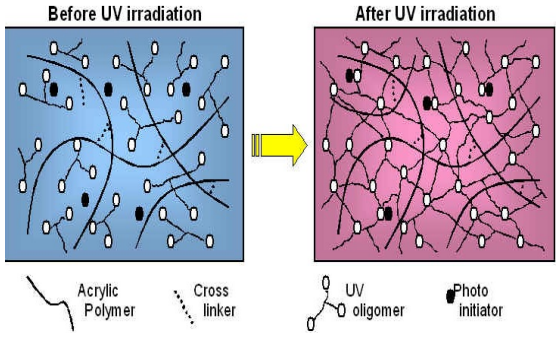

Fig. 4: The UV curable resist material formulation [40].

Additionally, material composition also includes sensitizers [41] (to improve UV light

absorption), surfactants [42] (for example fluorinated surfactants to reduce their adherence to the mold), more than one photoinitiator [43] (to increase cure speed), and finally solvents (to be able to adjust the thickness of the spin-coated layer) [44].

There are many examples of UV-NIL material formulations. The Epoxies[45], vinyl ethers[46] and acrylates appear to be the most popular materials used for this purpose because of their commercial availability and ability to photocure rapidly [38].

Many institutes such as Nanonex (e.g. NXR 2000 and NXR 3000), Molecular Imprint, AMO (e.g. Amonil), Obducat (e.g. STU®), micro resist technology (e.g. mr-UVCur 21), Shell Chemicals (EPON SU-8 epoxy resist) etc. have developed UV curable reists for commercial use.

1.6 Polymer deposition

For resist deposition onto the substrate techniques such as spin coating, spray coating, drop-on demand coating and droplet dispense can be used. The applied coating technique is strongly dependent on the desired film thickness. The high resist film thickness homogeneity as well as the short coating times make spin coating the most-applied coating technique.

A typical spin coating process as shown in Figure 5, involves depositing a small amount of a fluid resin onto the center of a substrate and then spinning the substrate at high speed.

In general, there are two common methods of dispense i.e. static and dynamic dispense. In the static dispense process, a small amount of solvent is simply deposited on the center of the substrate, before the spin process starts. On the other hand, the dynamic dispense process implies solvent dispersion while the substrate is turning at low speed.

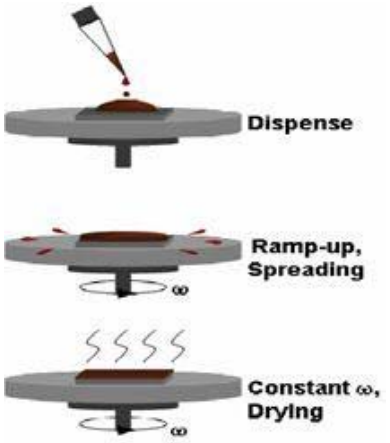

Fig. 5: Overview of the spin coating process. A solution is applied to the center of a flat substrate. The spin coater rotates the substrate with high speed in order to spread the fluid by the centrifugal force. A thin layer of polymer remains on the substrate [47].

In general, there are two common methods of dispense i.e. static and dynamic dispense. In the static dispense process, a small amount of solvent is simply deposited on the center of the substrate, before the spin process starts. On the other hand, the dynamic dispense process implies solvent dispersion while the substrate is turning at low speed.

After the dispense step, it is common to accelerate to a relatively high speed to thin the resist to near its final desired thickness. The resist film thickness attained by spin coating represents the equilibration between centrifugal force and solvent evaporation, both increasing with spin speed. In principle, higher spin speeds and longer spin times create thinner films[48]. Typical spin speeds for this step range from 1500-6000 rpm and from 10 seconds to several minutes, depending on the substrate size as well as the properties of the fluid such as viscosity, drying rate, percent solids, surface tension etc.

The remaining solvent concentration in the resist film also impacts its thickness. During coating, the solvent concentration drops and saturates at a value of approx. 15-25 % which depends on the film thickness and is higher for thicker films. The subsequent soft-bake reduces the remaining solvent concentration to values of 5 %. Furthermore, high ambience solvent saturation in the spin coater reduces the attained resist film thickness due to a suppressed solvent evaporation from the resist. Therefore, the first few wafers of a coating series might reveal a slightly higher film thickness as compared to wafers subsequently coated with a certain amount of fresh resist in the spin-coater [49].

1.7 Surface Characterization

1.7.1 Atomic force microscopy (AFM)

Atomic Force Microscopy (AFM) was developed for measuring the topography of small regions in a sample. As shown in *Fig. 6*, the main components of AFM are a cantilever with an AFM probe (tip), a X/Y/Z scanner, and a Photo Sensitive Position Diode (PSPD).

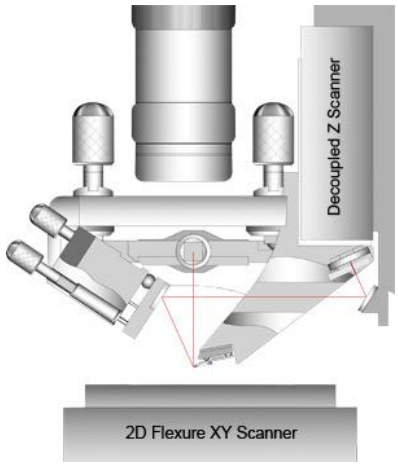

Fig. 6: View of AFM head [50].

The XY scanner is used to scan the area of interest on the sample surface. During the scanning, the AFM tip at the end of the cantilever very closely approaches the surface and interacts with the sample surface. The radius of curvature of the probe is in the nanometer range. The distance between the surface and the tip is dependent on the AFM modes i.e. contact, non-contact, or intermittent contact, set-point, etc. The interaction force between the sample and the tip deflects the AFM cantilever and the deflection is measured by PSPD. The Z-scanner is controlled to keep the interaction force (defined by set-point value) constant. The extremely low stiffness of the AFM cantilever enables the detection of the force below several nN. Information on the movement of the Z-scanner yields a topographic image of the sample surface [51].

1.7.2 Contact angle

In resist coating and imprint processes, the non-sticking and sticking phenomena between molds, resists and substrates are a well known problem to be considered. Surface chemistries and surface energies are the properties that cause such phenomena. Analysis of the surface properties can be performed using many methods. One of them is contact angle measurement.

When a small amount of a liquid is put in contact with a flat surface, the tri-phase boundary that separates the solid state of the substrate, the liquid state of the droplet and the vapor state, is known as the contact line (*Fig. 7*). If the substrate is chemically homogeneous and the surface is uniform, the contact line is a circle. The plane containing the normal of the solid surface and cutting through the apex of the liquid droplet is known as the meridian plane. The contact angle is defined as the angle between the solid surface and the tangent of the liquid at the tri-phase contact point in the meridian plane, through the liquid phase [52].

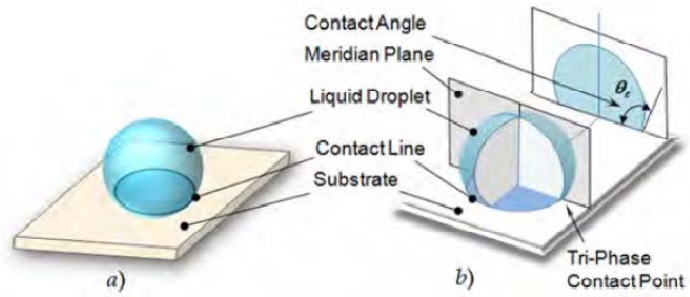

Fig. 7: A liquid droplet is placed in contact with a solid surface (a), and main features of the liquid droplet (b) [52].

For dynamic liquid droplets on surfaces, the amount of liquid put on the surface produces the large or so called advancing contact angle $\theta_a$which is the contact angle measured while the volume of the liquid droplet is increasing and the contact line is moving outwards, and the small one, or so called receding contact angle which is the one measured while the volume of the liquid droplet is decreasing and the contact line moving inwards. This phenomenon of existence of multiple contact angles for the same probe liquid is known as hysteresis. The difference between advancing and receding contact angles is defined as contact angle hysteresis.

The contact angle hysteresis provides information about roughness and chemical heterogeneity of the surface [52].

Alternatively, the degree that a surface is wetted by a liquid is defined as the wettability of the surface. Wettability describes the tendency for a liquid to spread on a surface. In practice, the wettability of a surface is evaluated by examining the profile of a probing liquid droplet which is put in contact with the surface, and characterized by contact angle. If the probing liquid is water and contact angle is less than 90°, a wettable surface is known as a hydrophilic surface, whereas an un-wettable surface is referred to as a hydrophobic with contact angles greater than 90° [52].

1.7.3 Autofluorescence

The nanoimprinted polymer surfaces manufactured in this project are used for optical biochip applications. Hence a low autofluorescence of the chip at the excitiation wavelength used is mandatory in order to reach a high sensitivity. A high autofluorescence may be an intrinsic property of the polymer used as well as a result of the optical properties of the nanostructures. Autofluorescence of the chip becomes important, since it may interfere with the signal of interest, often leading to suboptimal limits of detection. Typically, undesirable background interference or autofluorescence is a fluorescent signal originating from substances. Therefore, it is desirable to minimize all sources of autofluorescence in order to increase sensitivity of the chip.

1.8 Protein Microarrays

Within the last decade, high throughput approaches have been developed for the study of proteins, including profiling of proteins using mass spectrometry, tagging and subcellular localization and protein microarrays [53]. Protein microarrays are important high-throughput analytical tools in basic and advanced proteomic research, medical diagnostics and drug delivery. In proteomics, protein microarrays enable high-throughput parallel analysis of population profiles, biochemical properties and biological activity of proteins or peptides. In medical diagnostics, protein arrays offer a direct way to estimate the concentration profile of proteins and thereby diagnose disease state, stage and response to treatment. Protein

microarrays can also be used in drug delivery, since many drugs function by disrupting protein-protein interactions [54].

1.8.1 Assay Design: Immunoassay format

Depending on the field of application, protein microarrays can be classified into two categories: (1) Arrays for proteomics or focused protein profiling and (2) arrays for functional studies. The first category can be subdivided by array format into forward- and reverse-phase protein microarrays. The difference between the two refers to the way the sample is applied [55].

In the case of **forward-phase protein arrays**, the sample is incubated with the array so that different analytes can be detected simultaneously [56]. Examples include antibody microarrays that are used for the identification and quantification of target proteins such as sandwich, competitive and inhibition immunoassays.

Sandwich microarray format shown in *Fig 8*, requires two distinct antibodies capable of binding separate epitopes on the protein of interest [57]. The capture antibody which is specific for the target antigen and binds analyte from the solution is first immobilized on the chip surface. In the second step, the array is incubated with the detection antibody that binds to another epitope of the target antigen. This second antibody is labeled with a fluorescence indicator or alternatively with a biotin-streptavidin reporter system. The fluorescence signal is then proportional to the concentration; the more antigens are bound the greater is the signal that can be detected. This format requires standard curves of known concentrations of analytes to allow for quantification of the analytes [58].

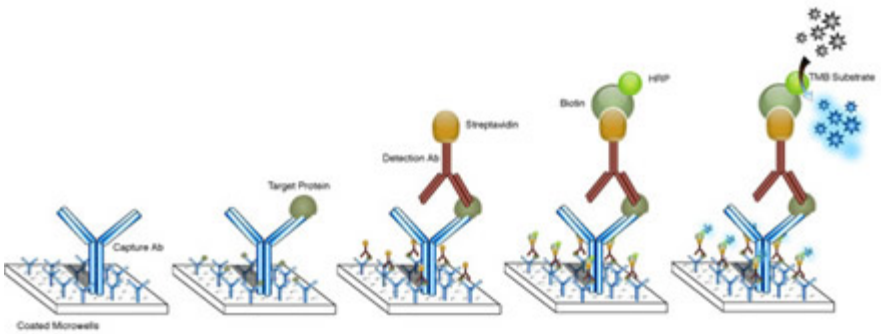

Fig.8: Processing steps of a sandwich assay [59].

In*competitive immunoassays***,** thecapture antibody is immobilized onto the chip surface while an unknown antigen and another labeled antibody are added in the solution. The antigen competes with a fluorophor labeled antibody to bind with the capture antibody. The response is then reversely related to the amount of analyte in the sample [60].

Furthermore, *Inhibition Immunoassays* use the ability of the analyte to inhibit the binding of the high molecular weight (MW) detecting molecule to the surface. Typically, the analyte is attached to the surface of the chip as a ligand, while the detecting molecule (added to the samples at a fixed, known concentration) is a macromolecule that binds specifically to the analyte. The mixture is then incubated and flown over the sensor surface to measure the remaining free detecting molecules. The amount of detected molecules is then inversely related to the concentration used for low MW analytes [61]. This assay format is often used to detect antigens with different MW presented in two different concentrations in one sample.

Reverse-phase arrays consist of different samples that are immobilized on a chip. In a single step, a large collection of probes can be screened for the presence or absence of one distinct target protein[62]**.** The RPA is suited for detection of differentially regulated proteins in healthy or diseased tissue and treated and untreated cells, the identification of disease-specific biomarkers, or the analysis of cell signaling networks [63].

1.8.2 Modification and Protein Immobilization

Assay design is a very critical issue because of the complex protein structure and sensitivity. Proper assay design includes the selection of a suitable chip substrate and immobilization strategy.

Various different chip substrates can be used for protein arrays such as fused silica, plastic, metal and glass surface [64]. The ideal chip substrates pose common attributes: theyprovide mechanical and thermal stability, and lowautofluorescence; enhance the signal to noise ratio of the analyte, limit non-specific binding and are cheap and compatible with different detection systems [57]. Furthermore, the choiceof immobilization strategies shall ensure a surface chemistry with low background noise. In addition, it is desirable to control orientation and adhering of proteins on/to a chosen chip surface, to allow retaining native biological activity of the protein [64] and protein accessibility by the target analyte in the

solution. Protein chip design offers a large range of immobilization approaches including covalent binding, adsorption and affinity.

Covalent binding is the most robust method for protein immobilization. This method relies on covalent bond between functionalgroups (e.g. –SH, -NH_2, -COOH) on protein molecules and other complimentary coupling groups (*e.g.* aldehyde or epoxide) on the solid surfaces[73]. The most robust approach to covalently immobilize proteins is to use aldehyde or epoxy-modified surfaces for covalent bonding to –NH_2 groups of a protein molecule.

Adsorption is a simple and effective immobilization technique often used in microplate immunoassays for large proteins due to their ability to form more contact points with the surface. Immobilization of proteins by adsorption can be performed in two ways: via electrostatic forces using e.g. aminosilane slides or via hydrophobic interaction on nitrocellulose membranes [54-55].

However, since the binding occurs only by adsorption this strategy often leads to denaturation of the protein on the surface, uncontrolled protein immobilization and thereby low protein binding and low signal intensity.

Affinity binding is used for uniform orientation of proteins on the chip surface. In this immobilization technique, for the attachment to the chip surface, protein probes are fused with a high affinity tag at their amino or carboxyl terminus [57]. One popular approach relies on surface immobilized protein molecules that recognize specific domains on antibodies. Oriented antibodies may be obtained using immobilized Protein A or G, which binds to the Fc portion of antibodies [58]. Another prominent approach is to use biotinylated antibodies on (strept)avidin coated surfaces to achieve orientation control.

1.8.3 Protein detection

Protein microarray detection techniques are classified as being label-based and label free.

Most of the microarray applications use fluorescence, chemiluminescence or colorimetric labeling strategies for detection of proteins.

Fluorescence labeling is based on the use of conventional dyes. In this regard, the use of cyanine dyes e.g. Cy3/Cy5, Alexa Fluor 547/647 and Dy547/Dy647 are the most common

fluorophors employed for protein microarray detection due to limited dye interaction, excellent brightness, and reduced complexity.

Chemiluminescent detection methods are based on Western blotting protocols for detection of antigen-bound antibodies with secondary antibodies conjugated to alkaline phosphatase or horseradish peroxidase.

The most employed label free methods are mass spectrometry and surface plasmon resonance. *Mass spectrometry* microarrays utilize a protein-selective surface for the immobilization of a complex protein solution. Ions liberated from the surface by laser desorption/ionization fly to a detector and are classified based on their mass/charge ratio [45]. *Surface plasmon resonance (SPR)* is based on the generation of the so-called surface plasmons. They are oscillations of the free electrons that propagate in the parallel to a metallic/dielectric interface, which allows measuring changes in the refractive index close to the sensor surface.

2 Experimental Section

In this chapter, master design profiles, preparation of stamps and deposition of anti-sticking and photoresist layers are introduced. A discussion about surface characterization techniques, assay design and fluorescence detection is also given.

2.1 Materials

Sylgard 184 silicone elastomer and curing agent were obtained as a kit from Dow Corning Corporation (Midland, USA). Vinyl PDMS prepolymer and Pt catalyst were obtained from ABCR GmbH, Germany. A modulator (2,4,6,8-tetramethyltetravynilcyclotetrasiloxane) was obtained from Sigma-ALDRICH, USA. Hydrosilane prepolymer was obtained from ABCR GmbH, Germany. SU-8 (Epikote 157), mr-IT85, Ormoprime 08 and Ormostamp material were purchased from micro resist technology (Berlin, Deutschland). Norland Optical Adhesive 72 and 75 was obtained from Norland Optical Adhesive, NJ. Amonil MMS 1 and MMS 10 resist was from AMO GmbH, Germany. Epon™ Resin 1002F was purchased from Miller Stephenson Chemical Co. (Illinois, USA) and was dissolved in cyclopentanone (Sigma) with a solid content of 10 wt.%. Bovine Serum Albumin (BSA) and microscope glass slides (J. Melvin Freed brand) were obtained from Sigma Aldrich, Germany. CRP antigene was purchased from Meridian Life science, Inc. USA. Monoclonal anti CRP C7/Dy647 (λex= 635 nm) and C7/Dy547 (λex= 635 nm) were obtained from Exbio, Czech Republic. Polyoxyethylen-sorbitan-monolaurat (Tween-20) was purchased from Sigma, USA. Tris (hydroxymethyl)-aminomethan (i.e. Tris) was obtained from Merck, Germany. CHAPS was obtained from Fluka Chemie, Switzerland. Phosphate buffered saline (PBS) was purchased from Invitrogen (USA).

2.2 Masters

Differently nanostructured surfaces themselves can provide a platform with increased surface area for protein immobilization and thereby enhance the sensitivity and selectivity of detection. In that context, the following masters of various designs and dimensions were tested: (i) a commercially available compact disc (CD) with line pattern (the height of the lines depends on the recorded data), (ii) a standard TGZ 2 grating (from MicroMasch, Estonia) for AFM tip characterization, (iii) TGZ 11 also a grating (from MicroMasch, Estonia)

for AFM tip characterization, (iv) Mustapha silicone master kindly provided by Mustapha Chouiki, EVG, (v) and a silicon master prepared by e-beam lithography (from Temicon, Germany) with nine pads. Each pad carries discs of varying diameter and spacing. *Table 2* below summarizes information about masters such as aspect ratio (defined as height/width), master design, the height, the period length and the width of the features.

Table 2: Comparison of the master specifications.

Master	Aspect ratio	Design	Height [nm]	Width [nm]	Period [µm]
Temicon	n.d.	Discs	100 ± 10	n.d	0.125-0.500
Mustapha	0.30	Pillars	135	412	1
CD	0.16-0.17	Lines	80-180	740	1.6
TGZ 2	0.06	Gratings	126	1830	3
TGZ 11	0.70	Gratings	1350	1724	10

2.3 Stamp Fabrication

For fabrication of replicas of master templates of various patterns, soft, hybrid and Ormostamp™ working stamp materials were tested. Using different stamp materials will allow us to compare the pattern transfer accuracy of different stamps and effect of differently structured surfaces on protein microarray performance. The properties of the materials used for stamp fabrication are summarized in *Table 3*.

Table 3: Comparison of the material properties used for stamp fabrication.

Materials	Elastic modulus [MPa]	Elongation at break	Hardness [MPa]	Curing
Sylgard 184 (sPDMS)	1.8	160	4.77	Temperature
Hybrid PDMS	8.2	7	0.02	Temperature
Ormostamp	650	Low	36	UV-light

Based on references fromFuard et al. 2008[65], Schmid el at [29] Choi & Rogers[26], micro resist technology[66].

2.3.1 Soft PDMS

The soft PDMS (sPDMS) was fabricated by using two liquid components, Sylgard 184 elastomer as the base and a curing agent. Both components were mixed well to a ratio of 10:1 by weight and centrifuged for 2 minutes at 3000 rpm in order to remove air bubbles. Once all bubbles were removed, CD, Temicon, TGZ 2 and TGZ 11 master templates were poured over with the degassed PDMS. The masters were then placed in a 90°C hot oven for 20 minutes to cure. After baking, a scalpel blade was used to separate manually the PDMS from the used master.

2.3.2 Hybrid PDMS

The two layer hybrid PDMS stamp was prepared as described by Odom et al.[27]. 3.4 g of a vinyl PDMS prepolymer, 18 µl of a Pt catalyst and a drop of a modulator (2, 4, 6, 8-tetramethyltetravynilcyclotetrasiloxane) were mixed and then degassed for 1 min by centrifugation at 3000 rpm. 1 g of a hydrosilane prepolymer was then gently stirred into this mixture and mixed with a plastic stick. Immediately after, a thin layer of hPDMS was spin-coated onto a master Mustapha template (1000 rpm, 40 s, 500 acceleration) and cured for 30 min at 60°C in an oven. Afterwards, a thin layer of Sylgard 184 PDMS (approximately 3 mm) was poured onto the *h*PDMS layer and cured for an hour at 60°C.

2.2.3 Ormostamp

Ormostamp- working stamps were fabricated by depositing 350 µl of the adhesion promoter (OrmoPrime 08) onto a glass substrate, spin-coated at 4000 rpm for 40 s and baked at 150 °C for 5 min. All masters were then glued (with double adhesive tape) to glass substrates to ensure good stability during the stamp fabrication process. Subsequently, a drop of Ormostamp material was dispersed on the masters using a pipette and covered with an OrmoPrime coated substrate. To prevent moving and smearing the Ormostamp material, OrmoPrime coated substrate was attached to another glass substrate using four paper clips and pre baked on hotplate at 150 ^{o}C for 2 min. The whole set up was then UV cured at 1000 mJ/cm ^{2} (λ =365 nm) using UV Stratalinker 2400 (from Stratagene, CA) and post-baked on a hot plate at 130°C for 10 min.

2.4 Anti-Adhesion layer

The deposition of an anti-adhesion layer was performed by the vapor phase deposition method described by Beck et al[34]. To do so, we build up an in-house instrumental setup for this process step (*Fig. 9*).

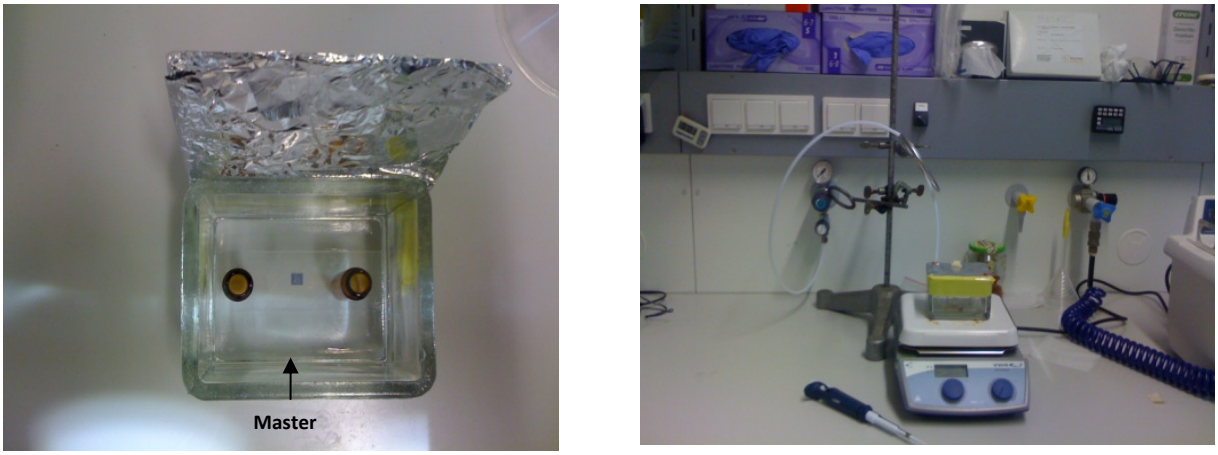

Fig.9: Instrumental setup for deposition of anti-sticking layer.

The master and/or Ormostamp were situated inside a glass container with two injection holes near the edge of the cover and placed onto a hotplate. The hotplate was heated to 250°C and after a while 10 µl of F3 -TCS was injected with a pipette through the hole. The injection hole was then immediately covered by a glue tape and the nitrogen was injected through the other orifice on the cover. In order for the gaseous molecules to come into contact and form covalent linkage with the master or Ormostamp surface, the master/stamp was left for 30 min in gas atmosphere.

2.5 Substrates and cleaning process

Microscope glass slides (75 x 25 mm) were used as substrates for all experiments. In general, cleaning processes consisted of an acetone, isopropyl alcohol (IPA) and deionized (DI) water clean for 10 min in an ultra-sonic bath. This removed all dust particles which were present on the glass surface. Eventually, all substrates were blown dry with nitrogen and baked at 200°C for 30 min to remove residual solvent.

2.6 Resists deposition

Thus, stability, reproducibility, operating parameters and behavior of the following resist materials were investigated: (i) SU-8, an epoxy-based resist, (ii) UV visible curing optical adhesives i.e. NOA 72 and NOA 75 (iii) mr-IT85 0.3 and mr-IT85 0.1 thermoplastic polymers suitable for low temperature NIL applications, (iv) mr- UVCur 21 as UV curable polymer, (v) Amonil MMS 10 as organic/inorganic composite UV curable resists for UV-NIL, and (vi) epoxy-based resin EPON 1002 F, a well characterized material,able to bind proteins via its epoxy function.

All experiments were conducted at room temperature. After the cleaning process described in section 2.5, the resist films were deposited onto glass substrates via the spin-coating technique. Spin coating was performed with the Modular Spin Processor WS-650-23 NPP (from Laurell).

The spin coating parameters for SU-8, NOA 72 and NOA 75 EPON 1002F and Amonil MMS 10 were adjusted through a series of experimental tests (see 3.14 and 3.1.6) while mr-IT85 0.1 and mr-UVCur 21 parameters on the other hand, were followed as recommended by the manufacturer's protocol.

2.7 Imprinting Process

Thermal and UV- NIL was realized using: EPON 1002F, mr-IT85 0.1 and Amonil coated substrates, and sPDMS and hybrid PDMS stamps replicas of the various masters.

As for the T-NIL process, the stamp was gently brought into contact with mr-IT85 0.1 and/or EPON 1002F coated substrates. The mold/mr-IT85 coated substrate assembly underwent thermal imprint process at 140° C for 2 min whereas EPON 1002F films were imprinted at 95 °C for 1 min on a hot plate. The embossed chips were then de-molded from the PDMS stamp at room temperature using tweezers.

As for the UV-NIL process, stamps were gently placed onto the Amonil coated substrate and cured by the UV light with a 200 W mercury lamp for 10 min through the transparent PDMS stamp. After the resist was polymerized by UV exposure, the Amonil coated substrate was completely separated from the stamp using tweezers.

2.8 Surface Characterization

Allstamps, coatings and imprints fabricated in this work were scanned using AFM (Nano Wizard II *from JPK Instruments*) operating in contact or intermediate mode. The aluminium coated silicon cantilevers such as CSC 38/AIBS for contact mode and NSC 35/AIBS for tapping mode (from *Micro Masch)* were used. All instrument parameters such as scan rate, integral and proportional gain and frequency of oscillation were adjusted separately for each sample. The AFM scans were further analyzed using the AFM software for image analysis (JPK Data Processing).

The initial thickness of the resulting coatings was determined by manually scratching the resist surface with tweezers, horizontally in the middle region of the sample with a constant pressure. The film thickness was then measured between coating and the produced scratch using AFM operating in intermediate mode in air.

To establish a dimensional profile of stamps and imprints, e.g. feature height (h), period length (p), width and surface roughness, were extracted from AFM cross section images.

To verify the wettability of produced chips, video based contact angle measurement method using a CAM101 video camera (*from KSV Instruments Ltd.*) was employed. In this implementation, the drop of water with a volume of 2 µl was deposited onto the sample using a pipette and then recorded by the videocamera at a speed of 40 framesper second. Afterwards, the KSV software was used to analyse the last recorded image with respect to base line, height, and shape of the droplet repeating the measurements at least three times. Contact angle values were obtained by averaging three measurements on different surface areas of the sample.

Additionally, autofluorescence measurements were employed to investigate optical properties of the imprinted materials. Autofluorescence was detected at two excitation wavelengths (λ_{ex}= 635 nm, λ_{ex}=532 nm) at a photomultiplier tube (PMT) setting of 1000 Volt using the GenePix™ 4000B non-confocal scanner (*from Axon Instruments*). Quantification of autofluorescence was performed with GenePix Pro 6.0 image analysis software. A grid of 25 x 25 spots with a diameter of 100 µm was placed on top of the imprinted area. The software

averages the pixel intensities within the round features. Mean values and standard deviation of the resulting 625 spot intensities were calculated.

2.9 Chip Processing

Each chip was incubated with 50 µl of CRP antigen with an end concentration of 1 mg mL-1 diluted in printing buffer 1x PBS/ 0.005% CHAPS/ 0.01% BSA ("cb"). To ensure complete probe immobilization, the chips were kept at 4°C for one week.

Surface blocking was performed for 30 minutes in 1x PBS (pH 7.2)/0.1 % Tween 20 in order to remove any unbound proteins and deactivate reactive surface groups. The slides were washed twice in 1x PBS (pH 7.2) at room temperature and dried using compressed air. Afterwards, the chips were incubated for 1 hour with 80 µl of Dy647-anti CRPand Dy547-anti CRP diluted with assay buffer (0.1 M Tris (pH 7.4), 10 mM $CaCl_2$, 100 mM NaCl + 0.1 % Tween) using five different concentrations i.e. 1.6 ng mL-1, 8 ngmL-1, 40 ng mL-1, 200 ng mL-1, 1000 ng mL-1. Incubation was carried out on a rotational shaker (The Belly Dancer (Stovall, Greensboro, USA) at room temperature. Finally, the slides were washed twice in 1x PBS (pH 7.2)/0.1% Tween and three times in 1x PBS (pH 7.2), dried using compressed air and scanned.

2.10 Fluorescence Detection

Fluorescenc*e* measurements (λ_{ex}=532 nm and λ_{ex}=635nm) were performed using the Genepix 4000B non-confocal scanner (Axon Instruments). For data comparison, the PMT gain was kept constant for each chip throughout scans. Image analysis was performed as described for the autofluorescence measurements in 2.9.

3 Results and Discussion

In the first section of this chapter 3.1, layer deposition followed by the replica molding results in 3.2 will be discussed. In section 3.3, the structuring of the EPON 1002F and mr-IT85 layers using T-NIL will be discussed, followed by a discussion on mold durability and repeatability. In section 3.4, the structuring of Amonil MMS 10 layers using UV-NIL will be presented, followed also by a discussion on mold durability and reproducibility. The optical properties of EPON 1002F and Amonil MMS 10 are described in section 3.5. The structured functional photoresist materials were then used as immobilization matrix in a protein microarray. In section 3.6, EPON 1002F assay performance will be discussed, followed by a discussion about assay performance using Amonil MMS 10 structured chips.

3.1 SPIN COATING

Our first specific challenge on the way to successfully fabricate polymeric nanostructured chips is to produce up to 100 nm thick and uniform resist layers over the whole substrate area. A number of parameters modulate resist thickness such as viscosity of the resist, temperature, spin speed, dispersion, contamination etc. The specific values for these parameters depend upon the equipment, the instrument settings and the resists that are employed [67]. Spin coating equipment described in 2.7 was used. Resist materials listed in 2.6 were tested in terms of behavior, stability, reproducibility and operating parameters. Fora resist to be considered as a suitable candidate for our NIL process, certain criteria must be fulfilled: first, it has to provide reproducible and highly uniform up to 100 nm thick films and secondly, films must be free of any deformations such as pinholes, streaks and bare areas on the substrate.

In order to optimize spin coating parameters and fulfil the requirements mentioned above, the effect of substrate cleanliness, cleanliness of dispense tip or pipette, presence of air bubbles in the resist as well as the effects of high and low temperature on film quality were investigated for each resist material. In that context, only glass substrates free from any dust and loose particles were used. Further, for resist deposition a new pipette tip was used for each sample. Moreover, in order to remove possible air bubbles, the resist materials were

centrifuged for 1 min at 3000 rpm prior to spin coating. In addition, surface wettability of resist films was estimated by contact angle measurements (see 2.9).

3.1.1 SU-8

In the series of experiments, 1% and 5% SU-8 resists were spin coated onto the glass substrates. Using a two-step dynamic spin coating program (see 1.6), different volumes were tested (i.e. 50 µl, 70 µl and 100 µl). Spin coating of 50 µl of resist volume produced non uniform layers characterized with bare edges and light streaked surface. To achieve better coating quality, we increased the material volume to 70 µl, and the spin coating speed was varied from 500 to 2000 rpm. However, every other repetitive try to produce consistent uniform films under the same conditions failed. By increasing the solvent volume to 100 µl no uniform films across the entire substrate were obtained either.

By contrast, coating three glass substrates with 70 µl of 5% SU-8 at 2500 rpm for 10 seconds followed by 3000 rpm for 30 seconds produced homogenous films. However, these results were not reproducible. In addition, contact angle measurements were performed. The contact angle was 77° ±0.2° for 1% SU-8 and 73± 0. 7 for 5% SU-8 indicating a hydrophilic surface of the coatings.

3.1.2 NOA 72 and NOA 75

In the case of NOA 72 and NOA 75, poor film quality was obtained. Therefore, this resist was excluded from further investigations.

3.1.3 mr-UVCur 21

The deposition of mr-UVCur 21 films included first deposition of a primer layer for adhesion improvement between substrate and resist and secondly, deposition of a top resist layer.

Firstly, following the manufacturer´s protocol, 150 µl of mr-UVCur 21 primer was spun onto the glass substrates. The primer coated surface showed defects. In attempt to improve surface quality, the volume of mr-UVCur21 primer per substrate was increased to 300 µl and excellent film uniformity was observed. Hence, the spin coating of 300 µl of mr-UVCur21 resist was straightforward. However, reproducibility of the conducted mr-UVCur21 coating

experiment was limited. In a 5 substrates cycle, only two uniform and defect free films were produced. In addition, the hydrophilic behaviour of the deposited mr-UVCur21 films was verified by static water contact angle measurements (54± 1.5°).

3.1.4. Amonil MMS 10

350 µl of Amonil MMS 10 resist was dispensed at the centre of a substrate in a static fashion (see 1.6) and a two-step spin coating program was performed; 3000 rpm for 40 sec to spread the resist along the substrate and 6000 rpm for 30 sec to determine the layer thickness were used. A sticky film surface with presence of pinholes was produced across the entire substrate. This might be a result of lacking cleanliness of the substrate, dispense tip or syringe, the presence of air bubbles in the dispensed resist, effects of high and low temperature and for the exposure to UV light. Thus, Amonil MMS 10 was centrifuged for 2 min at 3000 rpm prior to spin coating. The dispense pipette tip was changed after every dispersion. Perfectly clean glass substrates were used. Exposure of films to UV light using Stratalinker (i.e. 2 J/cm^2) subsequent to spin coating showed less effect on the smoothness of the films. Additionally, the use of a post-application bake at 60° C for 2 min significantly degraded the films. In order to study the effect of the lower temperature on the formation of pinholes and film quality, Amonil MMS 10 coated slides were stored in the refrigerator at 4° C for 2 days. No pinholes were visually evident and excellent film smoothness and quality was observed.

Next, film thickness was estimated by AFM. The resist surface was manually scratched with a tweezers and filmthickness was then measured between coating and the produced scratch. *Fig. 10* Illustrates Amonil MMS 10 scratched film as well as film cross section profile from which we estimated a film thickness of about 100 nm.

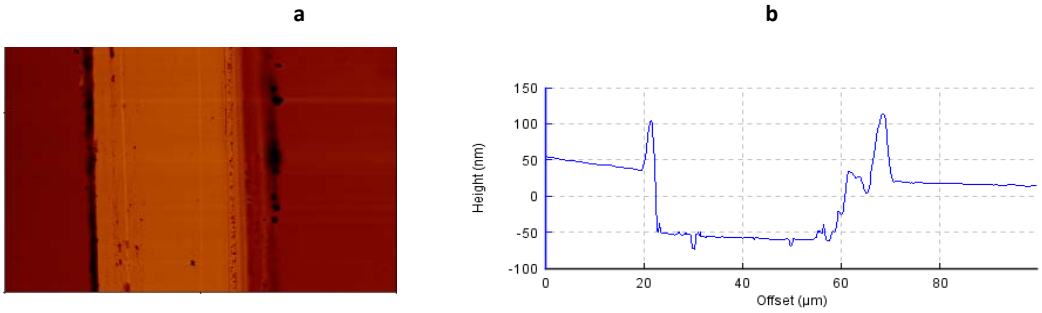

Fig. 10: AFM image of Amonil MMS 10 film with (a) one scratch and (b) cross section with an estimated thickness of approximately 100 nm.

Additionally, contact angle was measured and revealed hydrophilic behaviour (86 ± 0.3).

3.1.5 mr-IT 85

Spin coating of polymer mr-IT85 was performed by following the manufacturer's recommended protocol. 300 µl of mr-I T85 resist was spin coated onto the glass substrate at 3000 rpm for 60 sec. The substrates were then baked on the hot plate at 140°C for 2 minutes and allowed to cool. Afterword, the film thickness was measured using AFM as shown in *Fig. 11*.

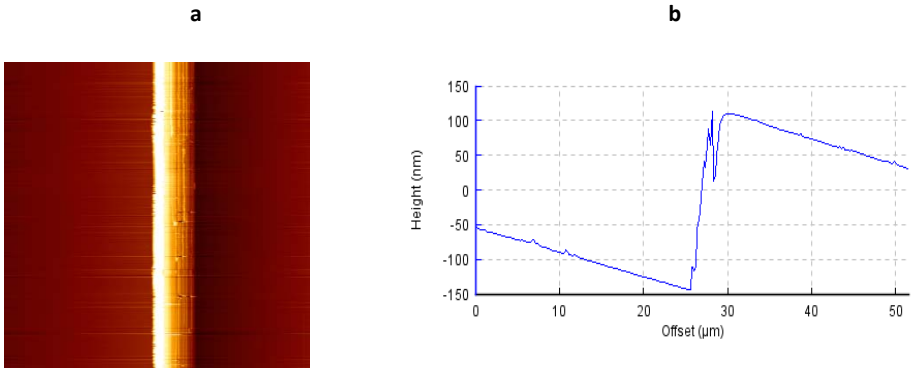

Fig. 11: AFM scan and cross section image of mr-IT85 film; (a) scratch, (b) and cross section image.

We measured the film thickness on two substrates. The initial film thickness was between 85-120 nm. Even though, the substrates are coated homogenously with no presence of any defects. In addition, a mean contact angle of 93° (SD= 1.4) across the entire sample indicated hydrophobic behavior of mr-IT85 films.

3.1.6 EPON 1002F

Spin coating of EPON 1002F was straightforward. All glass substrates were spun with 350 µl of EPON 1002F at 3000 rpm for 40 sec followed by 6000 rpm for 30 sec and excellent film quality was achieved. However, due to the hardness of the film (high cross linking density), we were unable to scratch the resist surface and measure corresponding film thickness. Further, contact angle of 81 ±0.6 showed hydrophilic behavior of the EPON 1002 coatings.

3.1.7 Summary

Our experiments showed that the non-uniformity of SU-8 films was neither affected by spin or ramping speed, time of spin, volume of solvent or acceleration speed. For this reasons SU-8 was not investigated further as resist material in this thesis, but rather served as a model system to get used to the technique. Further, NOA 72 and NOA 75 showed poor film quality. Therefore, these resists were excluded from further investigations. Additionally, due to unstable behaviour, the mr-UVCur21 was also excluded. Moreover, general framework for spin coating of Amonil MMS 10 resist was established. We produced uniform and highly reproducible coatings with a thickness of approximately 100 nm. Additionally, film quality was improved by storing the samples at 4° C right after spin coating. The spin coating of mr-IT85 was straightforward, fabricating uniform, from 85 nm to 120 nm thin films as well as spin coating of EPON 1002F whereexcellent film quality was achieved.

In conclusion EPON 1002F, mr-IT85 and Amonil MMS 10 fulfilled all criteria listed in 2.6 and were used for further NIL process.

3.2 STAMPS

The second challenge in fabrication of polymeric nanostructured chips is to produce compatible mold replicas. The stamp (mold) is one of the crucial elements of the NIL process since it determines the resolution of the features on the surface. A high-quality stamp exhibits smooth, straight sidewalls with sharp edges and precise geometry.

In this section, our goal was to produce high quality stamps using various stamp materials. We also aimed to understand and evaluate suitability of these materials for replication of different master designs based on the current state of knowledge about the replica molding technique. Master templates described in section 2.2 were replica molded using sPDMS, hybrid PDMS and Ormostamp materials as described in 2.3. All stamps were investigated by AFM. The AFM scans and corresponding cross section images were further analyzed with regard to feature's height (h), period (p), width (w), and compared to the master profiles. Besides, surface smoothness of the stamps was evaluated by extraction of the root mean square roughness (RMS) values from AFM scans by measuring each stamp at three different locations e.g. top, middle and bottom. The water contact angle (CA) values were measured at three different locations on the stamp. Average ± standard deviation values of CA are reported and discussed.

3.2.1 sPDMS Stamps

Different patterned soft PDMS stamps illustrated in *Fig. 12* were fabricated using a simple casting process described earlier in section 2.3.1. Due to elasticity of the sPDMS material, the stamp could be de-molded easily from the master template without any damages. *Fig. 12* a shows both, AFM scan and cross section images of the fabricated stamp and the original masters.

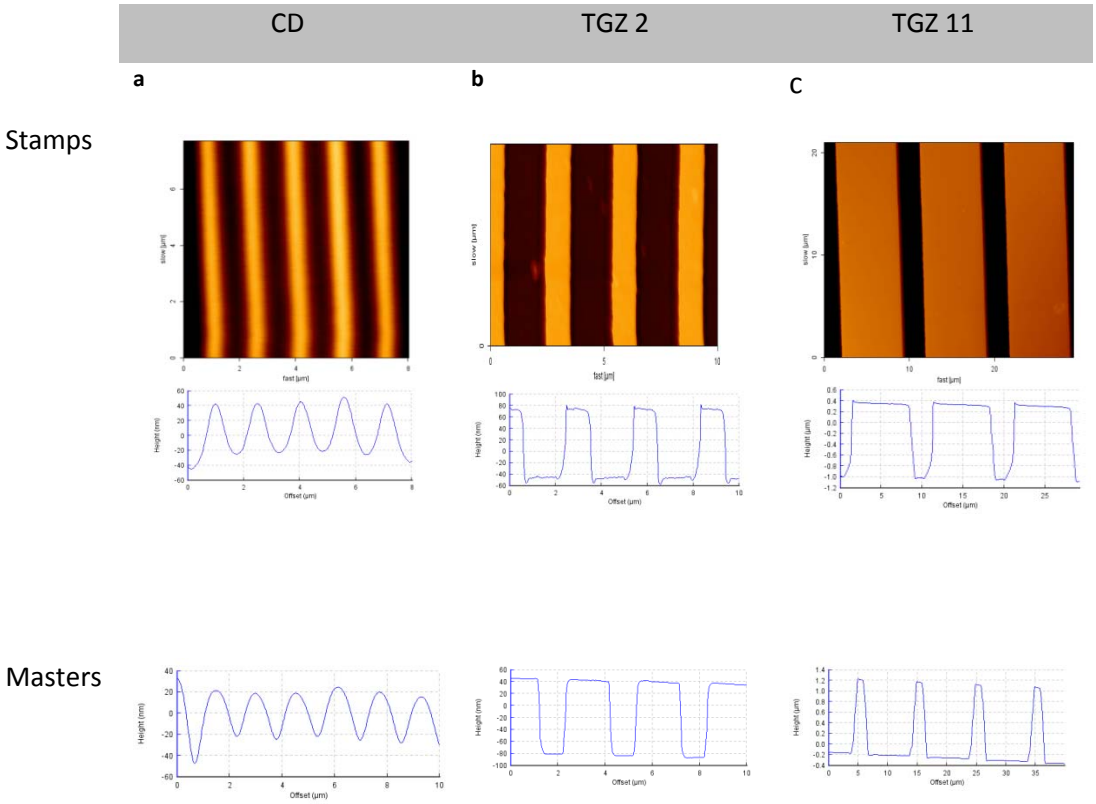

Fig. 12: AFM scans and cross section images of sPDMS stamps. Stamps were casted against (a) CD , (b) TGZ 2 and (c) TGZ 11 master templates.

Table 4 summarizes average and standard deviation values extracted from AFM cross section images for each fabricated stamp.

Table 4: The mean and standard deviation values of fabricated sPDMS stamps.

Stamp	Height [nm]	Periods [µm]	Width [nm]	Deformations	Contact angle [Θ°]	RMS [nm]
CD	127±2.6	1,6±1.2	745 ±1.7	No	136	41±0.4
TGZ 2	122±0.7	2,97±0.4	1116±1.1	No	108± 0.7	58±0.0
TGZ 11	1370±0.2	10 ±0.4	7250±1.8	No	n.d.	558±5.0

AFM investigations did not show any deformations of the CD in sPDMS replica (*Fig. 12a*). We report excellent agreement in features height and period length, slight increase in the width from 740 to 745 nm compared to the master mold. The surface of the stamp was smooth with RMS of 41 nm; CA (136°) indicates high hydrophobic properties.

Further, the gratings of TGZ 2 stamp correspond to gratings in the original master (*Fig. 12b*). The height of features is around 122 nm, the period approximately 3 µm and the width of features in the middle is 1116 nm, respectively. Data indicate 3% reduction of height and width caused by shrinkage during the PDMS curing step. The degree of shrinkage of PDMS (0.5 –2.5%) depends on several factors including curing temperature and time[70]. The curing parameters for our experiment were 90°C for 20 min. We assume that using lower curing temperature and longer curing time would contribute to even higher accuracy of the stamp. The roughness of the stamp is 58 nm and the CA (108°) shows hydrophobic behavior.

Lastly, the gratings of TGZ 11 stamp correspond well with the original master design (Fig. 12c). AFM measurements revealed slight increase of height by 20 nm and unchanged period length of 10 µm. Besides, high increase in the width of the features from 1.7 to 7.2 µm is measured in the middle. The roughness of the stamp is 558 nm, respectively.

The feature broadening observed for CD and TGZ 11 patterns can be attributed to the release of stresses in the bulk of the PDMS after its peeling off from the substrate surface [68]. The attempt to produce sPDMS replica molds of the Mustapha master failed. The sPDMS material was sticky and hence replication was not possible.

3.2.2HybridPDMS Stamp (sPDMS/hPDMS)

By combining the methods of 'standard' PDMS and h-PDMS, a composite hybrid PDMS stamp as illustrated in *Fig. 13* was fabricated using a simple casting process described earlier in chapter 2 section 2.3.2. Two master templates were casted i.e. Mustapha and TGZ 2. The TGZ 2 master was casted with hybrid PDMS material and used as a model system to get used to the technique and become aware of problems during fabrication. Since Sylgard 184 PDMS was not suitable for replication of Mustapha master, the template was casted with hybrid PDMS stamp material. After curing, thin PDMS stamp was easily separated from the Si

master substrate. All stamps were further analyzed with regard to the features height (h), period (p) and width (w). AFM scans and cross section images in *Fig. 13* offer comparison of the stamps with the original master profile.

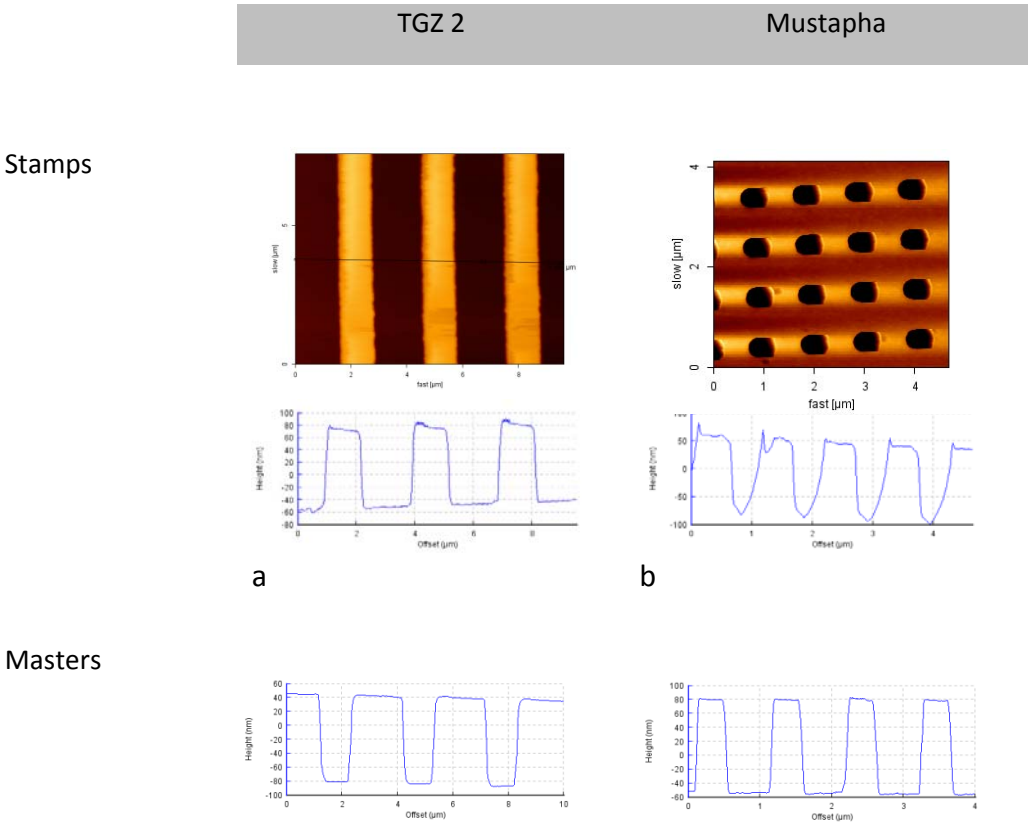

Fig. 13: AFM images of hybrid PDMS stamps casted against (a) TGZ 2 and (b) Mustafa master templates.

Table 5 summarizes mean and standard deviation values extracted from AFM cross section images for two fabricated hybrid stamps.

Table 5: The mean and standard deviation values of sPDMS /hPDMS stamps.

Replica	Height [nm]	Periods [µm]	Width [nm]	Deformations	RMS [nm]
TGZ 2	125±0.2	2,93	1232	No	59±0.0
Mustapha	130±11.0	1,04	688±35.0	Yes	54±3.0

The parameters of the TGZ 2 replicated structures on the PDMS stamp are consistent with the template (*Table 5 and Table 2*). *Fig. 13b* shows AFM images of the hybrid stamp pillars

and the cross section of the master Mustapha. The pillars of the stamp correspond well with the holes in the original master. The pillars on the stamp have rounded roofs (cross section image in *Fig. 13b*), which can be related to stresses during the curing process. However, despite the rounded roof of the features, the stamp profile was accurate with the Mustapha master design. Pillars with a height of 130 nm, 1 µm period and ~690 nm features width were obtained, indicating small features broadening during the peel off process. But these differences between master and PDMS replica may also be attributed to AFM scanning artifacts caused by blunt tips or high scan speed.

3.2.3 Ormostamps

Next, the replica molding process capabilities of the hybrid polymer Ormostamp was tested. Two different designs were replicated, i.e. Temicon and Mustapha pillars, and TGZ 2 and TGZ 11 gratings. The accuracy of the replication was verified by AFM inspection of the Si masters and the mold replicas. AFM cross section images of each, the Si master structure and the mold replicas are shown in *Fig. 14* together with the measured values summarized in *Table 6*. Average contact angles measured on three different locations on the stamp are also included.

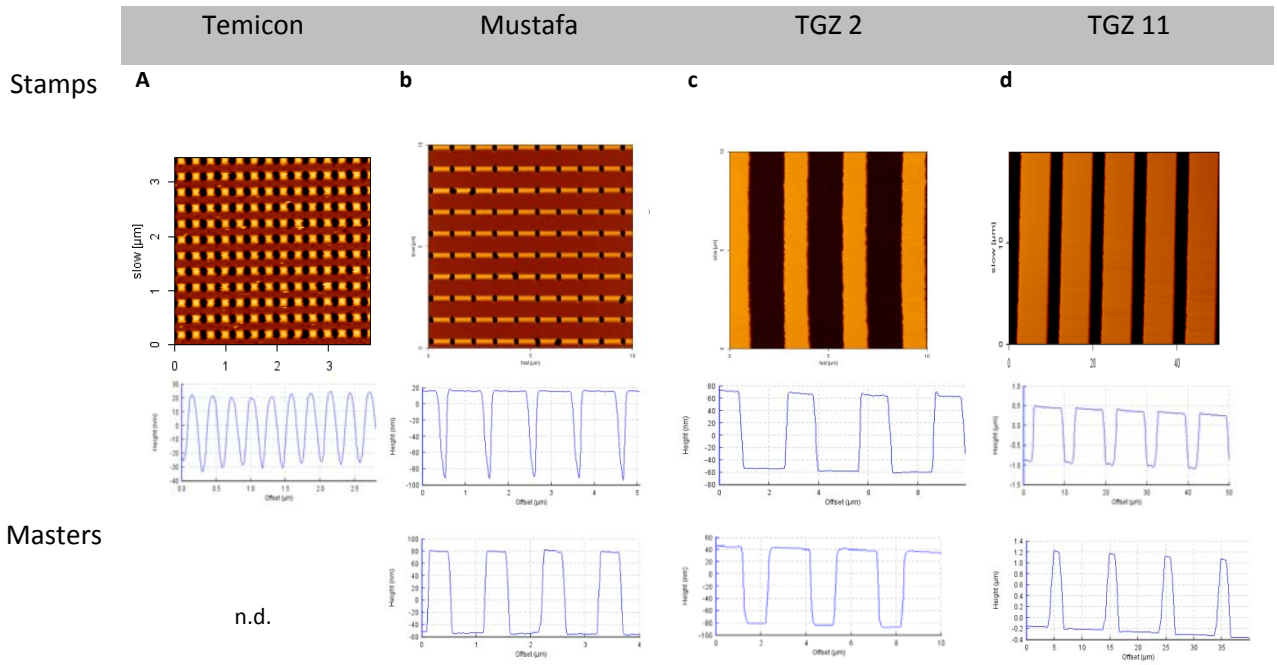

Fig. 14: AFM images of Ormostamp cured against (a) Temicon, (b) Mustafa,(c) TGZ 2 and (d) TGZ 11 master templates.

Table 6 summarizes average and standard deviation values extracted from AFM cross section images for all fabricated Ormostamps.

Table 6: The mean and standard deviation values of fabricated Ormostamps.

Replica	Height [nm]	Periods [µm]	Width [nm]	Deformations	CA [Θ°]	RMS [nm]
Temicon	45±7.0	0.125	n.d.	No	103 ± 1.3	19±0.8
Mustapha	110	1	881±13.0	No	89 ± 4.3	33±0.7
TGZ 2	126	3	1196±0.0	No	73 ± 4.5	60±0.1
TGZ 11	1380	9,3	7215±0.1	No	94 ± 3.8	565±0.1

Fig. 14 shows AFM images of Ormostamp fabricated from Temicon master. Please note that the Temicon master consists of nine different pads with varying disc diameter (the height is 100 nm for all 9 pads) and spacing profiles. The pillars from the stamp correspond to the pillars in the original master (pad B2, with height of 75±10 nm and periods of 200±10). The height of features is around 45 nm and the period approximately 125 nm, indicating a reduction of 40 % in height and 38 % in periodicity of the pillar patterns on the stamp.

AFM images of Ormostamp replicated from Mustapha master are illustrated in *Fig. 14 b*. The pillar's structural shape from the stamp corresponds to the holes in the original master. The height of pillars is 100 nm indicating a decrease by 25 nm compared to the master. The period length of 1 µm correlates well with the periodicity of the original master. Further, the width of around 880 nm indicates pillars broadening. Surface roughness is 33 nm; contact angle (89 °) implicates a more hydrophilic behavior of the stamp surface.

Fig. 14c shows AFM images of Ormostamp fabricated from TGZ 2 master. The gratings from the stamp correspond well with the grating structures in the original master. Constant and homogenous height, periodicity and homogeneity of the fabricated features were observed, indicating an excellent agreement with the master profile. Further, surface roughness is around 60 nm; the contact angle (73 ± 4.5) indicates hydrophilic behavior of the stamp surface.

Ormostamp fabricated from TGZ 11 master template is shown in *Fig. 14d*. The height of pillars is 1.3 µm and the width is 7.2 µm, indicating an increase, which probably can be related to stress during cross linking of Ormostamp material. Further, periodicity between pillars is slightly decreased by 700 nm; surface roughness is 565 nm.

In addition, CA of stamps was measured at room temperature before and after deposition of the anti-sticking layer (see 2.4). *Table 7* presents contact angle mean ± standard deviation values calculated from three measurements per stamp.

Table 7: Surface energy values of the Ormostamps measured before and after deposition of the antisticking layer.

Stamp	Without anti-sticking layer	With anti-sticking layer
Temicon	103±1.3	113±1.5
Mustapha	89±4.3	116±2.7
TGZ 2	73±4.5	104±2.0
TGZ 11	94±3.8	106±2.0

Before deposition of the anti-sticking layer, all stamps showed more hydrophilic surface behavior. Upon deposition the stamps turned hydrophobic as represented by the increased contact angle which was enhanced by up to 30°.

3.2.4 Summary

Several molds with micro- to nanoscaled features of various sizes and shapes were fabricated by the replica molding technique using three different mold materials. The suitability and transfer accuracy was studied. Based on our data, Sylgard 184 PDMS molds fabricated from CD, TGZ 2 and TGZ 11 masters were demonstrated in defect free and high-fidelity pattern transfer. Further, small variations in the width of the replicated patterns were observed, even though the general shape was maintained.

Hybrid PDMS stamps were used for replica molding of TGZ 2 and Mustapha masters. Both types of the stamps were successfully fabricated. Since TGZ 2 master was also replicated by Sylgard 184 PDMS material, in comparison, our data suggest higher transfer accuracy of TGZ 2 master template by using the hybrid PDMS stamp material.

In addition, using Ormostamp material, the working stamps of Temicon, Mustapha, TGZ 2 and TGZ 11 were faithfully fabricated. The stamps are of high quality and exhibit straight and vertical sidewalls. The best transfer accuracy was achieved using TGZ 2 master. Furthermore, Ormostamp and hybrid PDMS stamp materials were used for replica molding of the master Mustapha. In terms of transfer accuracy, hybrid PDMS turns out to be the better choice. Further, advantages and drawbacks for both of the mold materials were found. In comparison, the advantage of hybrid PDMS material is rapid fabrication and high accuracy of pattern transfer. On the other hand, Ormostamp material showed high structural quality transfer of the pillar patterns.

Lastly, no significant difference in transfer quality was observed using Ormostamp and Sylgard184 PDMS for replica molding of the TGZ 11 master template. Both stamp materials were applicable for a high quality pattern transfer. However, sPDMS was favorable due to its simple preparation, rapid fabrication and low price.

3.3. THERMAL IMPRINTS

By now, uniform, resist layers as well as differently patterned stamps were fabricated and inspected in the section 3.1 and 3.2. The next step in the fabrication of polymeric nanostructured platforms is the imprinting process. Understanding and controlling the imprinting process is crucial for efficient and reliable pattern transfer from the mold into the coated substrate by means of Nanoimprint Lithography.

In this section, T-NIL imprinting process was used for the structuring of EPON 1002F and mr-IT85 homogenous surface layers. A detailed description of the T-NIL principle was previously given in chapter 1, section 1.1.1. Film deposition details are given in 2.7. and 3.1. It should be noted that it was impossible to determine the EPON 1002F film thickness due to the hardness of the resist layer. Final thickness of mr-IT 85 films was between 85 - 120 nm. The stamps used for the imprinting process were described and discussed in 3.2. The imprint process was explained in chapter 2, section 2.8. Imprint temperatures of 95°C for EPON 1002F and 140°C for mr-IT85 films were used. The topography of the patterned samples was examined by AFM. The pattern fidelity between the mold and the imprinted features was investigated using four parameters: height (h), period (p), width (w), and root mean square roughness (RMS provides information about the accuracy of pattern transfer and the vertical size of the roughness of the surface texture [71]). AFM JPK software is used to accurately extract these four metrics by using AFM cross sections at three different random positions over the imprinted nanostructures and calculate mean and standard deviation. Estimated imprint profiles were further compared to the corresponding stamp profile. In addition, the static water contact angle (CA) of the imprinted surface was measured.

3.3.1 EPON Imprints using sPDMS mold

In the first experiment, four differently patterned masters i.e. Temicon, CD, TGZ 2 and TGZ 11 were tested. Examples of various imprinted patterns are depicted in *Fig. 15 (a-d)*.

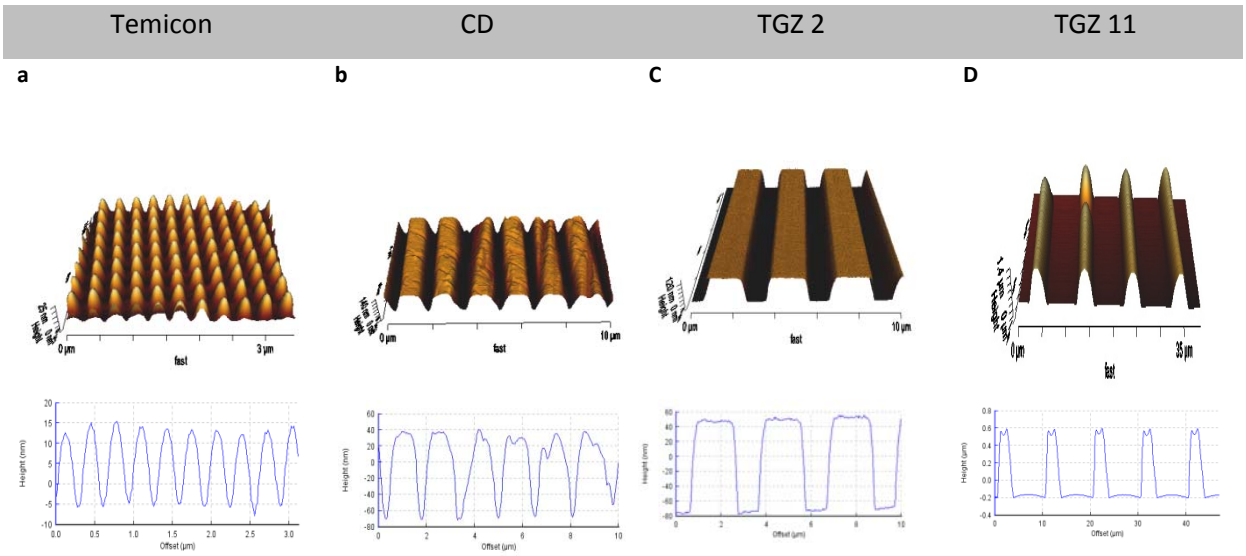

Fig. 15: AFM images of the imprints using (a) sPDMS Temicon , (b) CD, (c) TGZ 2 and (d) TGZ 11 molds.

Table 8 summarizes average and standard deviation values extracted from AFM cross section images for the imprints performed using various sPDMS molds.

Table 8: Mean and standard deviation values for EPON 1002F imprints.

Imprint	Height [nm]	Periods [µm]	Width [nm]	Deformations	Contact angle	RMS [nm]
Temicon	20±4.0	0.211±8.0	n.d.	No	103±1.3	7±0.2
CD	108±2.7	1±1.8	1015±0.7	Yes	86.5±1.2	36±0.6
TGZ 2	120±1.2	3±0.4	1866±0.1	No	108±0.0	55±0.1
TGZ 11	2100±0.6	10±0.7	2365±0.1	Yes	105±0.7	371±1.0

Fig. 15a illustrates AFM scans and cross section images of an imprinted resist using Temicon replica in sPDMS. The stamp was brought in contact with the coated substrate and no pressure of any kind was applied.

Please note that it was impossible to scan Temicon sPDMS stamps due to technical problems. Therefore, in order to access the accuracy of the imprinted patterns, the imprint profile was compared with the original master profile i.e. Temicon master pad B2 with the height of 75 ± 10 nm and the periodicity of 200 ± 10 nm. An array of sub 75 nm pillars was faithfully replicated. The imprinted pillars have a mean height of around 20 nm, and the mean periods of ~211 nm. Based on our data (*Table 8*), a reduction by 73 % in height of the imprinted pillars was obtained. The transfer accuracy can most likely be improved by applying pressure on the top of the stamp during imprinting, thereby assuring better and conformal contact between the stamp and substrate. In addition, imprint time could be increased to allow the resist to fully fill the cavities of the stamp. Still, homogenous and excellent pattern structure (*Fig. 15a*) was observed. Further, surface roughness is 7 nm, while contact angle (103°) indicates a more hydrophobic surface of the imprint.

AFM scan and cross section image of the CD imprinted lines are depicted in *Fig. 15 b*. The imprint was performed using 1.5 x 1 cm CD mold replica in sPDMS as depicted in *Fig. 12a* with a height of 127 nm, period length of 1.6 µm and line width of 745 nm (*Table 4*). No sticking problems occurred during de-molding due to the hydrophobic character (136°) and the elasticity of the PDMS. After bringing the stamp in contact with the substrate, we observed formation of small air bubbles between stamp and substrate. Trapped air bubbles result in a disrupted pattern. Therefore, the backside of the stamp was gently stroked with a tweezers, removing air bubbles and resulting in more uniform contact. AFM cross section image in *Fig. 15b* shows patterns with partial roof deformations. This is probably caused by too strong adhesion between the stamp and the surface during the detachment step. Despite damaged roofs, it can be seen from *Table 8*, that fine lines of approximately 108 nm in height were faithfully duplicated. Further, a decrease in period length of 1 µm and increase in features width to 1 µm were measured. The contact angle measurements (86°) implicate hydrophilic behavior of the imprint surface. The surface roughness is 36 nm.

AFM images in *Fig. 15c* show uniformly imprinted grating structures. The imprinting was performed using TGZ 2 mold replica in sPDMS as depicted in *Fig. 12b* with the height of 122 nm, period length of 2.9 µm and line width of 1.1 µm (*Table 4*). To assure better contact with the substrate pressure was manually applied on the stamp by using tweezers, but was not

kept constant during the imprint process. The patterns with sharp, vertical and smooth edges similar to the original stamp with a height of 120 nm, and a period length of 3 µm were faithfully imprinted. A broadening by about 700 nm of the gratings was observed even though the general shape is maintained. Further, RMS roughness was decreased by 3 nm; contact angle of 108° implicates hydrophobic behavior of the imprint surface.

In *Fig. 15d*, the images of an imprinted grating of a TGZ 11 mold replica in sPDMS *(Fig. 12c*) are given. The backside of the stamp was gently stroked with a tweezers to remove air bubbles and assure better contact with the substrate. Sagging of the grating structures was observed. This typical phenomenon of PDMS was discussed in 1.3. Further, 43 % increased height (*Table 8*), unchanged period length of 10 µm and reduced width of features from 7.2 µm to 2.3 µm were measured by AFM. Further, the surface roughness is 371 nm;the contact angle is 105° implicating hydrophobic behavior of the imprint surface.

3.3.1.1 Reproducibility and sPDMS mold durability

Both imprint lithography process repeatability and mold durability are essential in making imprint lithography a useful manufacturing technology[12]. Reproducibility of the imprinting process is typically affected by the chosen stamp material, imprinting resist and applied nanoimprint technique. In this context, we performed detailed reproducibility studies using sPDMS stamps replica of CD, TGZ 2, TGZ 11 and Temicon masters, EPON 1002F films and the T-NIL technique. For a mold to be defined as highly reproducible and durable the following two criteria have to be met:

- first, at least seven out of ten imprinted substrates need to match the master mold profile in terms of texture and geometry and
- secondly, imprints must not reveal any pattern deformations such as sagging, pairing and buckling.

The pattern accuracy between the mold and the imprinted features was investigated using three parameters: height (h), period (p), and root mean square roughness (RMS). AFM JPK software is used to accurately extract metrics values out of AFM scanning images. AFM cross section has been measured at three different random positions over the imprinted nanostructures. The mean and standard deviation values of the three measurements are calculated and used to build the height, periodicity and RMS profiles. Estimated imprint profiles were further compared to the corresponding stamp profile. Besides, several studies point out that changes in surface roughness impact the wettability in a certain way depending on the nature of the surface [72]. To investigate the correlation between surface roughness and wettability of the imprinted surface, accurate contact angle measurements were performed.

CD stamp

EPON 1002F coated substrates were thermally imprinted with a sPDMS stamp of a CD master. The same stamp was used for all imprint cycles. The stamp was neither removed for cleaning nor for inspection purposes to avoid contamination. The AFM cross section images shown in *Fig. 16* compare the structural quality of the first and the last imprint, using the same mold.

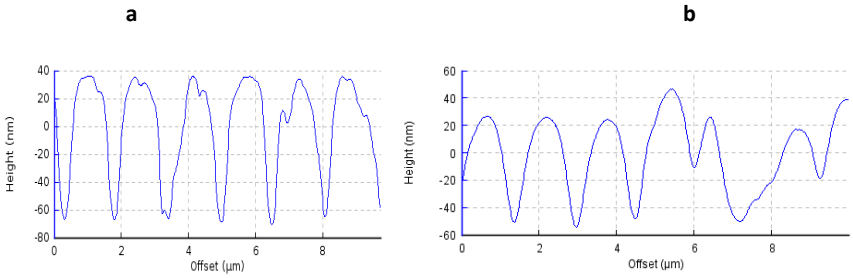

Fig. 16: AFM cross section profiles of CD imprints for the (a) first and (b) last imprint.

Eight out of ten EPON coated substrates were thermally imprinted with the same sPDMS stamp replica of CD. *Fig. 16a* shows minor roof defects probably caused during demolding. Further pairing or lateral collapse of the features can be seen in *Fig. 16b*. *Latteral collapse* occurs when the closely spaced features adhere to each other laterally due to high capillary forces [30,31]. As a consequence, an increase in periodicity was recognized for the imprint shown in *Fig. 16b. Fig. 17* plots period length against number of imprints. The red line shows the estimated period length of the CD stamp i.e. 1.6 µm.

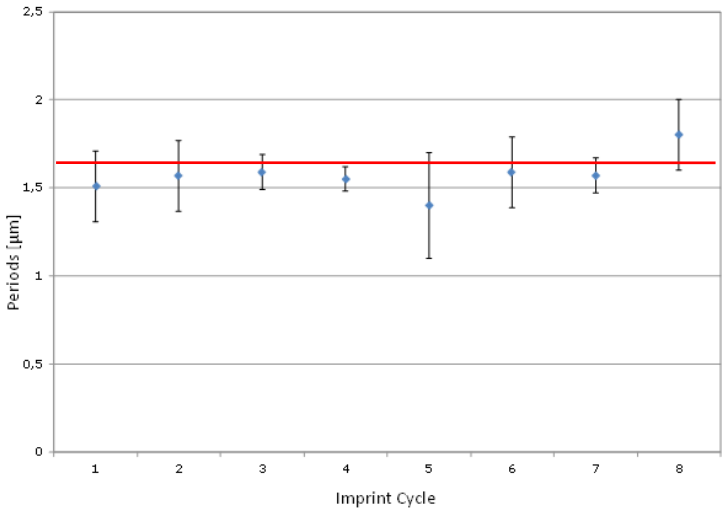

Fig. 17: Periodicity profile with mean and standard deviation values measured during the course of 8 imprinting cycles.

Otherwise, during the first seven circles, periodicity is mostly decreased compared to the stamp profile. The same decrease was also observed in the height profile. *Fig. 18* plots measured heights of nanostructures against number of imprints. Please note the red line indicating the height of the sPDMS stamp i.e. 127 nm.

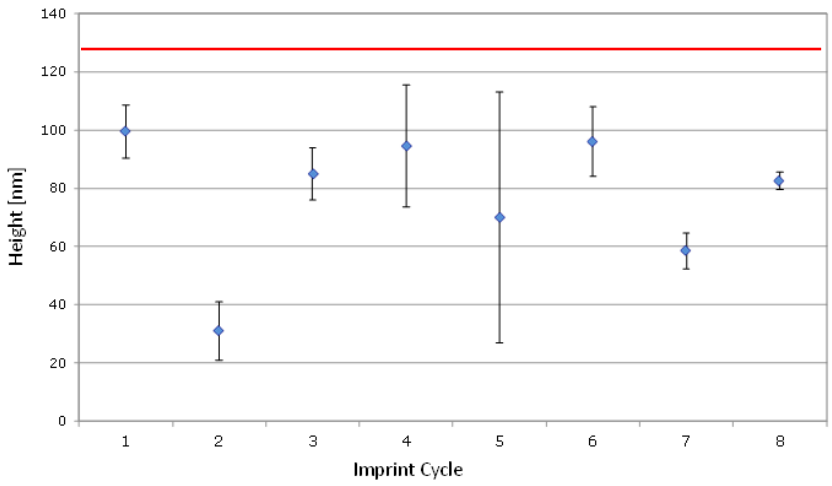

Fig. 18: Height profile with mean and standard deviation values.

Compared with the stamp profile, reduction in the height of the features was observed. Variations in pattern height were probably caused by non-uniformity of the film thickness. Further, the surface roughness (RMS) values of each imprint were measured as indicator for surface roughness and accuracy of the imprints. RMS of the stamp is 41 nm (red line in *Fig. 19*).

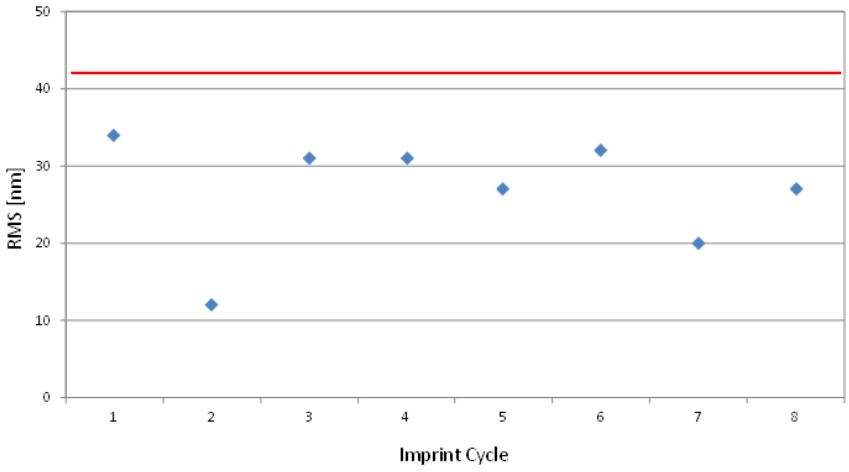

Fig.19: Surface roughness profile with mean values for eight CD imprints.

RMS roughness is reduced compared to the stamp profile. This implicates a smoother surface of the imprinted features. We also found a good correlation between surface roughness and measured height of the patterned lines. Data point distribution of RMS (*Fig. 19*) and estimated height profile (*Fig. 18*) show identical pattern.

This correlation implicates that a decrease in roughness of the imprinted surface is related to reduce height of the imprinted lines and non-accurate imprinting. CA values illustrated in *Fig. 20* represent measurements obtained for five CD imprints and five resist films exposed to temperature. We note that CA of resist film after spin coating was 81° ± 6°.

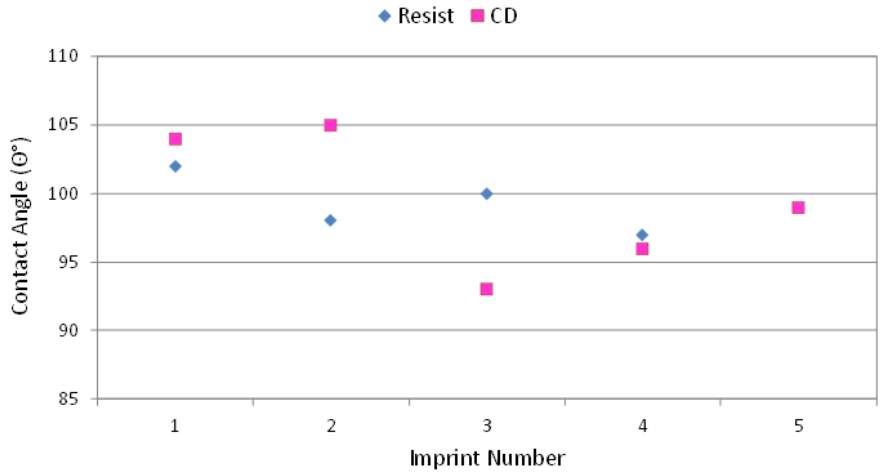

Fig. 20: Wettability profile with mean and standard deviation values for five CD imprinted substrates.

As is obvious, hydrophobicity of the resist film is increasing with temperature. The surface of the imprints is also more hydrophobic than the non-structured surface after spin-coating. In addition, to clarify the impact of the surface roughness on wettability of the imprinted surface, the RMS values in *Fig. 19* and CA values in *Fig. 20* were compared. We found that smoother surfaces provide better wettability of the imprints.

Finally, imprinting eight out of ten EPON coated substrate characterized with high structural deformation of the features implicates limited repeatability and durability of the CD sPDMS stamp.

TGZ 2 Stamp

Another set of EPON 1002F coated substrates was imprinted with TGZ 2 replica in sPDMS. The same stamp was used for all imprint cycles. The stamp was neither removed for cleaning nor for inspection purposes to avoid contamination. The AFM cross section images shown in *Fig. 21* compare the structural quality of the first and the last imprint, using the same mold.

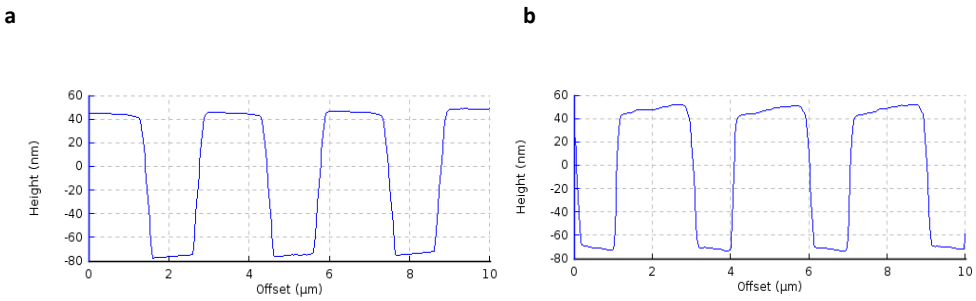

Fig. 21: AFM cross section profiles for the (a) first and (b) last imprint.

All ten substrates were faithfully imprinted. Looking at the cross section pictures in *Fig. 21*, we see that the grating structures were uniformly distributed. No deformations were observed. The height profile given in *Fig. 22* reveals minor variations compared with the stamp profile. The red line indicates the height of the stamp i.e. 122 nm.

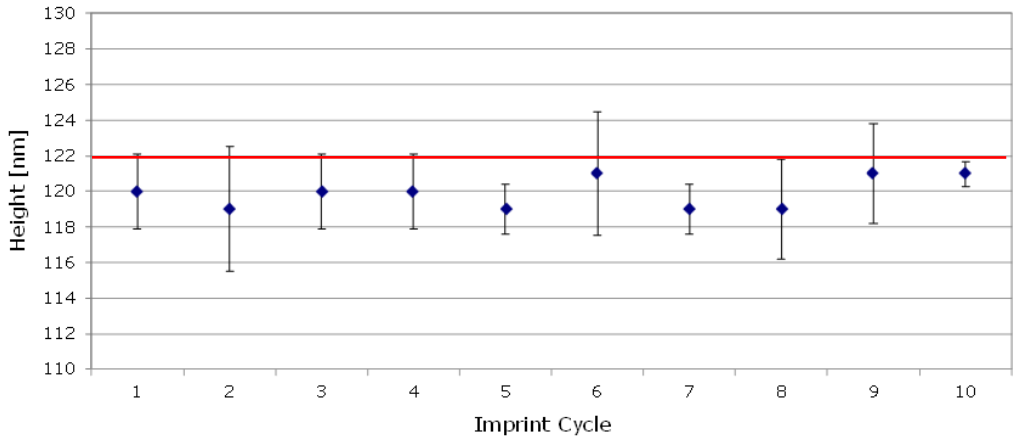

Fig. 22: Height profile for TGZ 2 imprints with mean and standard variation values.

Lower height values, ranging from 119 to 121 nm were obtained during ten imprint cycles. On the contrary, unstable periodicity was estimated and shown in *Fig. 23*. The red line implicates the estimated period length of the TGZ 2 stamp i.e. 3 µm.

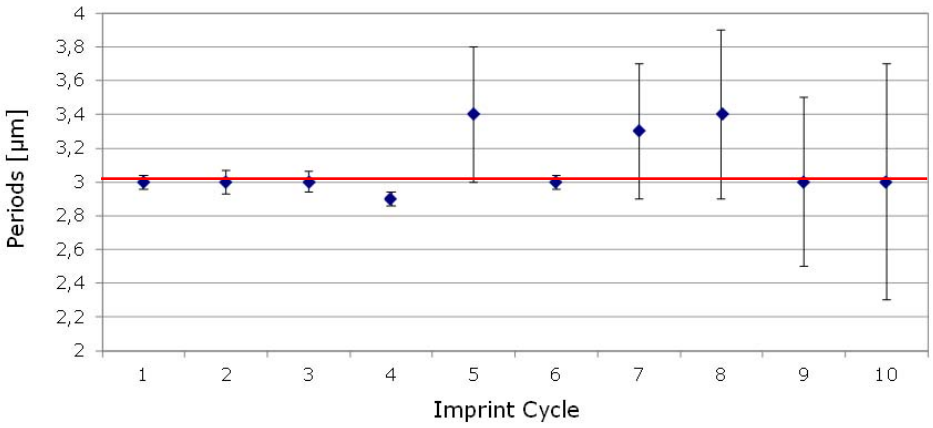

Fig. 23: Periodicity profile for TGZ 2 imprints with mean and standard variation values.

For the first four imprints, stable periodicity of about 3 µm was observed, matching the stamp profile. Further, the period length is irregularly increased and highly deviates between no. 5 and no. 8 (*Fig. 21*), while for imprint no. 9 and 10, periodicity is similar to the mold profile of 3 µm. Further, lower RMS values were achieved (*Fig. 24*) for the imprints than for the stamp (58 nm).

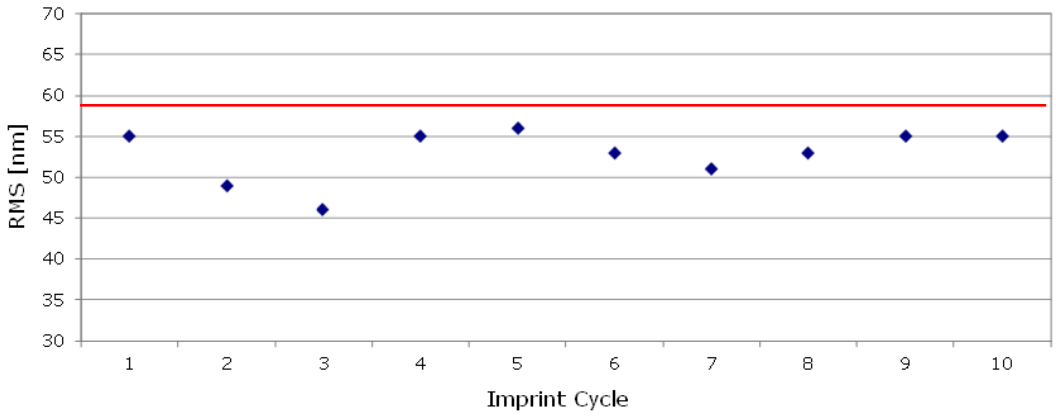

Fig.24: RMS profile for TGZ 3 imprints with mean values.

Through AFM inspection we did not see a major difference in surface roughness between our stamps and imprints. All imprints had slightly decreased mean roughness of a few nm following the surface roughness of our initial Si master stamp. After ten imprints, no increase of the imprinted line roughness is observed, meaning that no significant degradation of our working stamp appears at this stage.

Further, almost identical profile between surface roughness (*Fig. 24*) and measured height (*Fig. 22*) of the patterned lines can be seen. This correlation implicates that the decrease in roughness of the imprinted surface is related to the reduced height of the imprinted lines. In addition, average CA values illustrated in *Fig. 25* indicate hydrophobic behavior of the imprinted surface.

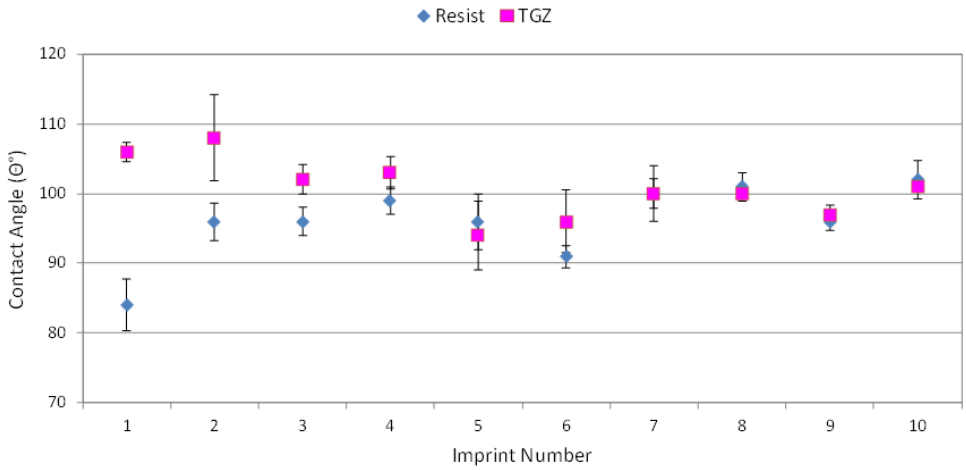

Fig. 25: Wettability profile for TGZ 2 imprinted substrates.

It can be seen that the CA of the imprints is higher compared with the CA of the plain, non-structured resist. Further, by comparing RMS and CA (*Fig. 24 and Fig. 25*) our results implicate that smooth imprinted surfaces are more hydrophobic.

Finally, thermal nanoimprint lithography, has proved an excellent technique for imprinting sPDMS mold replica of TGZ 2 onto EPON 1002F films. Ten out of ten high quality substrates with defect free grating and minor deviation compared to the stamp were imprinted, implicating excellent mold durability and reproduction of sub 120 nm features.

TGZ 11 Stamp

Next, reproducibility of TGZ 11 replica in sPDMS onto EPON coated substrates was investigated. The same stamp was used for all imprint cycles. Five out of ten samples were evaluated. The AFM cross section images shown in *Fig. 26* compare the structural quality of the first and the last imprint, using the same mold as discussed in 3.2.1.

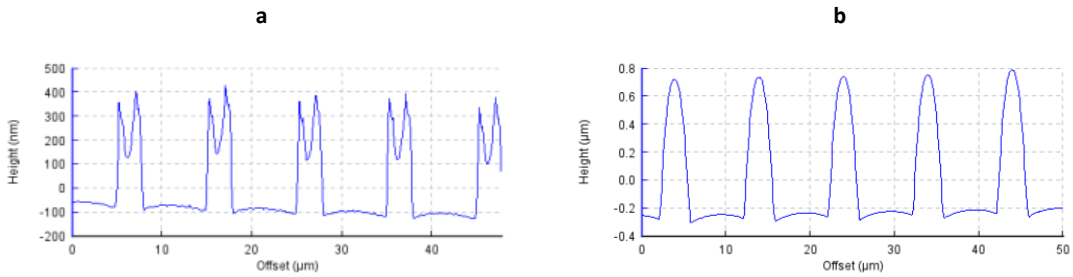

Fig. 26: AFM Cross section images of the (a) first and (b) last imprint.

Roof collapse of imprinted gratings was observed for the first four imprints. On the contrary, the cross section of the last imprint (*Fig. 26b*) shows well defined and uniform grating structures. It is to be noted that we were not sure about having scanned the same region on each sample. It is possible that the stamp was already partially damaged during the fabrication process and that those damages are registered by AFM in this experiment. It is also possible that these deformations are a result of AFM artifacts.

In *Fig. 27* the height profile with mean and standard deviation values vs. number of imprint cycles is presented. The red line indicates corresponding height of the stamp i.e. 1.37µm.

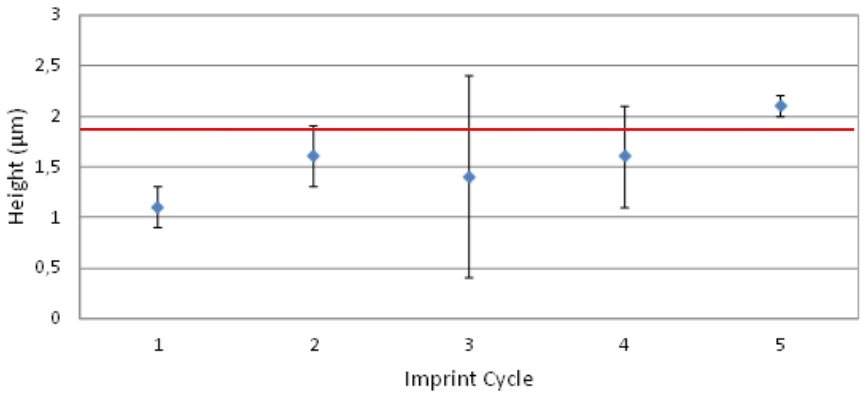

Fig. 27: Height profile for TGZ 11 imprints with mean and standard deviation values.

AFM measurements revealed a variable height profile for the TGZ 11 stamp and mismatch between the stamp and imprinted gratings. *Fig. 28* illustrates period length vs. imprint cycles. The red line implicates the estimated period length of the TGZ 11 stamp i.e. 10 µm.

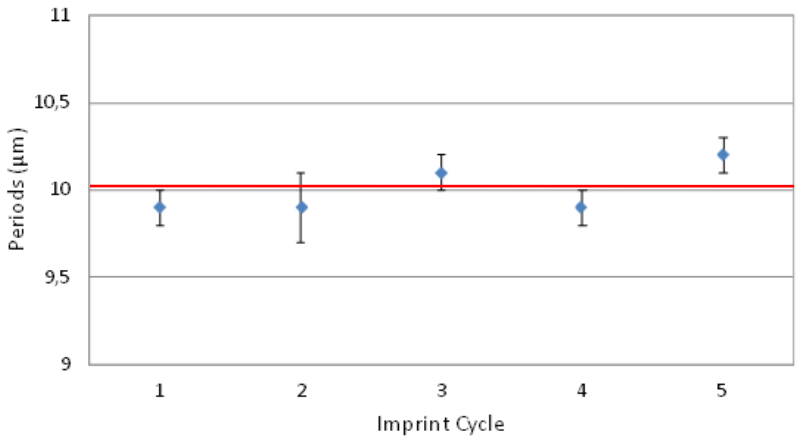

Fig. 28: Periodicity profile for TGZ 11 imprints with mean and standard deviation values.

We observed stable periodicity of the TGZ 11 imprints, matching the stamp profile. Further, *Fig. 29* shows RMS profile measured for five imprinted substrates. RMS of the stamp is 558 nm. Reduced RMS values were estimated for imprinted substrates, compared to the stamp asdepicted in*Fig. 29*.

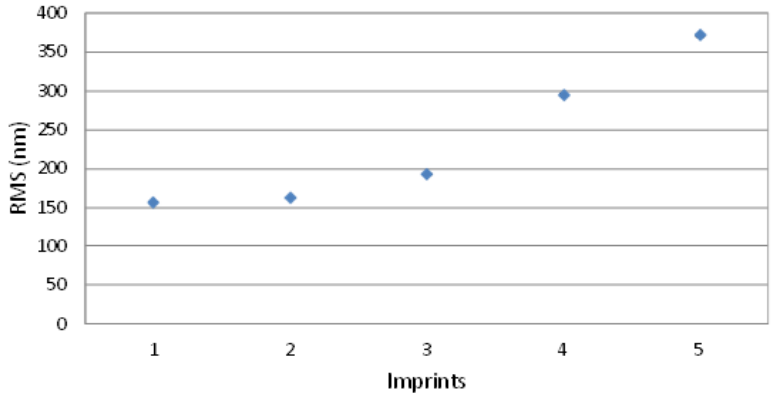

Fig. 29: RMS profile for TGZ 11 imprints with mean values for five imprinted substrates.

As is obvious from*Fig. 29*, surface roughness of the imprints increases exponentially during the course of 5 imprinting circles. Besides, good correlation between the RMS and height profile was observed. As can be seen from *Fig. 27 and Fig. 29,* the height of the grating structures increases with increasing surface roughness. These findings confirm the poor accuracy of the imprinted TGZ 11 grating features.

Thus, our results implicate limited repeatability and durability of the TGZ 11 sPDMS stamp. In addition, the water contact angle (117°) revealed hydrophobic properties of the imprinted surface.

Temicon stamp

The durability of Temicon replica in sPDMS during T-NIL was investigated. The same stamp was used for all imprint cycles. As previously mentioned, it was impossible to scan Temicon sPDMS stamps. For that reason, imprints were only examined by AFM and investigated for the stamp durability purposes. No pressure of any kind was applied during the imprinting step. The AFM cross section images shown in *Fig. 30* compare the structural quality of the first and the last imprint. Please note that only one pad per imprint is scanned, randomly.

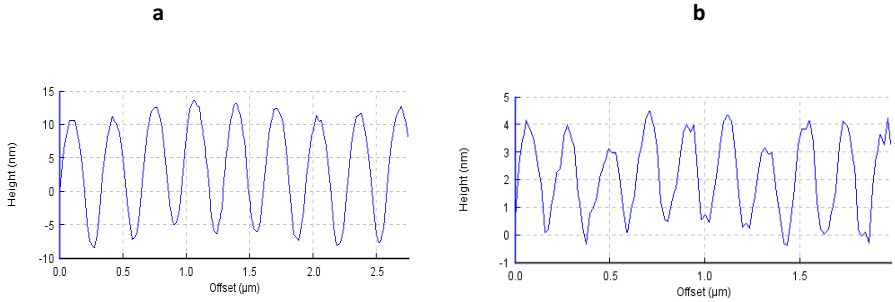

Fig. 30: AFM cross section of Temicon imprints: (a)first imprint, (b) last imprint.

Eight out of ten substrates were successfully imprinted. The cross section image in *Fig. 30a* illustrates high quality imprinted pillars with a mean height of ~13 nm and a mean periodicity of ~310 nm. Low values of the average RMS (7 nm) indicate a very smooth surface of the imprint. *Fig. 30b* shows pillars with an average height of ~4 nm and average spacing of 212 nm and RMS of 2 nm. Some features are slightly damaged probably during the demolding step.

The smallest pillar size on the original master is 75±10 nm. Our data shows high –resolution sub 10 nm imprinted pillars. Moreover, regarding accuracy, we assume that high reduction of the height compared to the master template is a consequence of imprinting without applying pressure. Anyway, some authors for example Trimbach et. al[69] argue that the use

of soft PDMS for high resolution patterning is limited in terms of reproducibility and pattern accuracy. On the contrary, our results show that good mold durability and repeatability as well as high imprint quality can be achieved using Sylgard 184 PDMS stamps for sub 75 nm thermal imprinting.

3.3.2 EPON 1002F imprints using hPDMS mold

Hybrid stamp replica of Mustapha master discussed in 3.2.2 was imprinted onto EPON 1002 F film via the T-NIL method. Please note that the final resist thickness of EPON 1002F coating is unknown. The stamp discussed in 3.2.2 was used. Imprint temperature was 95°C for 1 min. The imprint was further investigated by AFM operated in contact mode. AFM scans and cross section images are illustrated in *Fig. 31*. AFM scans were further analyzed with regard to features height (h), period (p), width (w) and root mean square (RMS). The average and standard deviation values of height, periods, width, RMS and CA summarized in *Table 8* were collected by measuring each imprint multiple times. Estimated imprint profiles were further compared to the corresponding stamp profile. Contact angles, a measure for surface wettabilitywere obtained by averaging three measurements on different surface areas of the sample. An example of Mustapha imprinted patterns is depicted in *Fig. 31*.

	Mustapha
Imprint	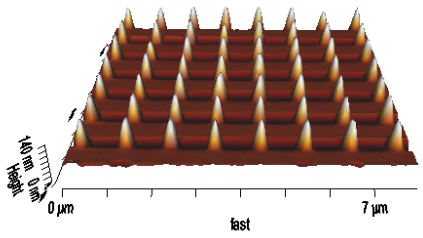 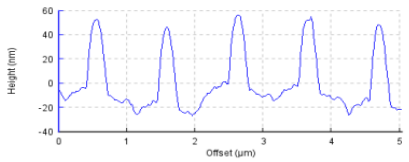
Stamp	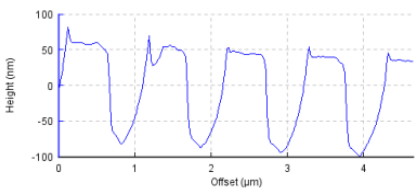

Fig. 31: AFM images of EPON 1002F film imprinted with Mustapha hybrid PDMS mold.

Table 9 summarizes average and standard deviation values extracted from AFM cross section images for the fabricated Mustapha hybrid stamp.

Table 9: The mean and standard deviation values of the imprint.

Imprint	Height [nm]	Periods [µm]	Deformations	Contact angle	RMS [nm]
Mustapha	69±9.0	1±0.4	Yes	108±1.7	22±5.0

An array of pillars was replicated. However, imprint profile does not agree well with the stamp profile. The height is reduced by 70 nm, while spacing between pillars remain unchanged i.e. 1 µm. Further, shape deformation of nanostructures was observed. It is evident from the cross section image in *Fig. 31* that resists build up in between the pillars. This indicates a reflow of resist. Longer imprinting time most probably allows the resist to spread more uniformly around the pillars.

3.3.2.1 Reproducibility and hPDMS mold durability

Reproducibility of Mustafa replica in sPDMS/hPDMS onto EPON 1002F coated substrates was investigated. The same stamp was used for all imprints. Pressure was applied on the top of the mold using tweezers to remove air bubbles but was not kept constant during the pressing process. Five out of ten samples were evaluated. Given in *Fig. 32* is height profile with mean and standard deviation values. The red line indicates the height of the stamp i.e. 130 nm.

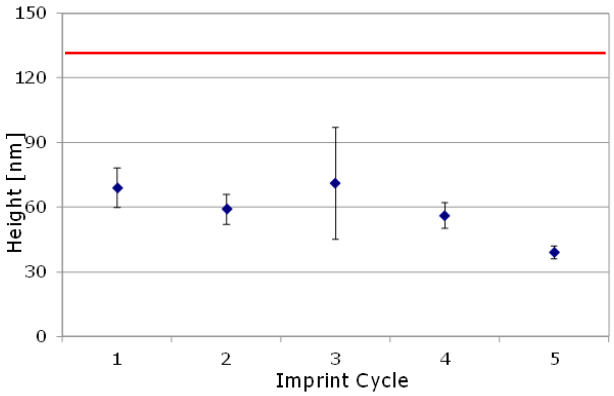

Fig 32: Height profile of the Mustapha imprints with mean and standard deviation values.

The height of the structure is homogenously reduced and different from the stamp profile. This loss is probably related to limited flow of the resist during imprinting also visible in *Fig. 33*.

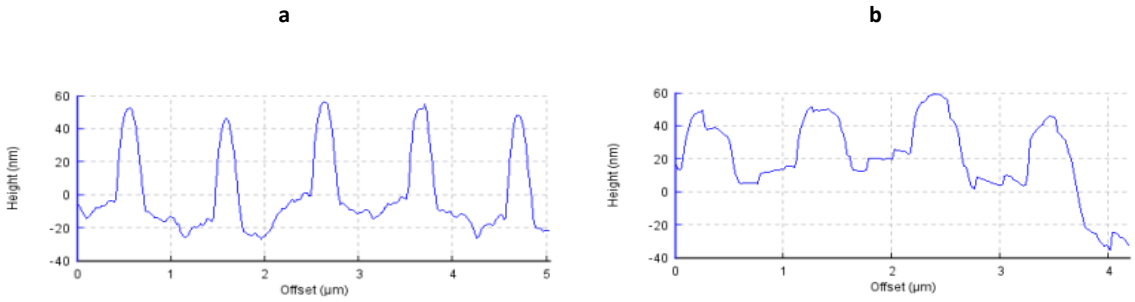

Fig.33: AFM cross section images of the (a) first and (b) last imprint.

Fig. 33 a-b showssignificant structural deformations, characterized by a loss of the original pattern shape. Further, *Fig. 34* illustrates period length profile for seven EPON 1002F imprints. The red line implicates the estimated period length of the CD stamp.

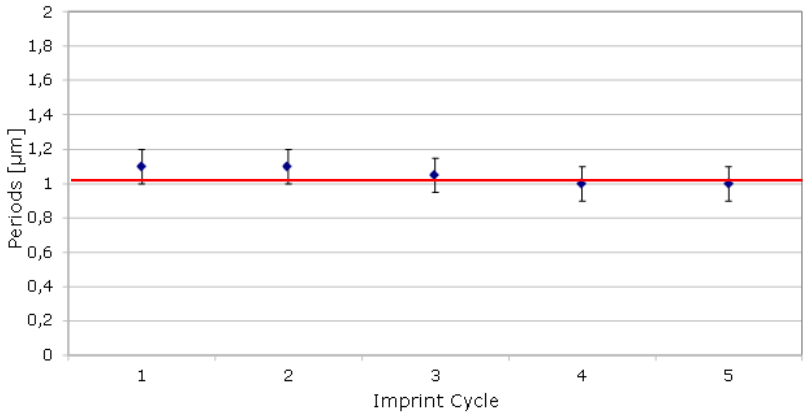

Fig. 34: Periodicity profile of the Mustapha imprints.

For the first three imprints, small increase in features spacing of 1.1 µm was observed. In the case of imprint no. 4 and no. 5, the spacing of 1 µm matches well with that of the stamp. In addition, measured CA showed hydrophobic behavior (102° ± 2) of imprinted pillar patterns.

3.3.3 mr-IT85 imprints using sPDMS molds

CD and TGZ 2 replica in sPDMS were imprinted in mr-IT85 films via the T-NIL method. Resist film thickness was 85 nm. The CD stamp (1 x 1.5 cm) has line patterns, where the height is 118 nm, the separation 1.6 µm. The TGZ 2 stamp has a periodic grating structure with a height of 120 nm, and a separation of 3 µm. Prior to imprinting, surface wettability of the stamps was determined. To do so, mean contact angles were calculated from three measurements on different surface areas of the stamp.

Imprinting temperature was 140°C for 2 min. Pressure was applied on the top of the mold by tweezers to remove air bubbles, but was not kept constant during imprinting. All Imprints were scanned and evaluated by AFM. AFM scans and cross section images are illustrated in *Fig. 35*. AFM scans were further analyzed with regard to features height (h), period (p), width (w) and root mean square (RMS). The average and standard deviation values summarized in *Table 10* were collected by measuring each imprint AFM scan multiple times. Estimated imprint profiles were further compared to corresponding stamp profile. In addition, the static water contact angle (CA) was measured. Contact angle values were obtained by averaging three measurements results on different surface areas of the sample. Examples of various imprinted patterns are depicted in *Fig. 35*.

	CD	TGZ 2
	a	**b**
Imprints	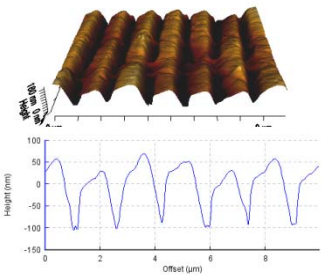	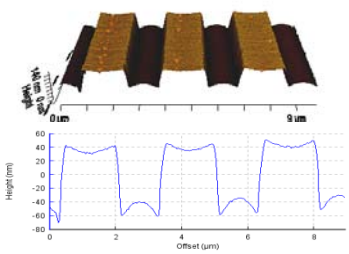

sPDMS Stamp c d

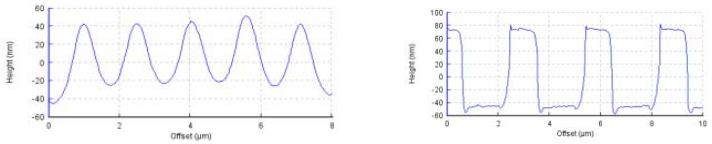

Fig. 35: AFM scans and cross section images: (a) CD imprint, (b) TGZ 2 imprint, (c) CD stamp cross section profile and (d) TGZ 2 stamp cross section profile.

Table 10 summarizes average and standard deviation values extracted from AFM cross section images for imprinted features.

Table 10: Average and standard deviation values of the imprinted mr-IT85 films.

Imprint	Height [nm]	Periods [µm]	Width [nm]	Deformations	Contact angle	RMS [nm]
CD	111 ± 7.6	1,6	1233	Yes	98±1.0	46 ±0.3
TGZ 2	90±1.0	1,9	1721	Yes	113 ± 4.0	47±1.2

Analyzing the AFM images of the CD imprints, the line structures (111 nm average height), and period length (1.6 µm) match well the stamp profile. We observed sharp straight roofs of the features (*Fig. 35a*) and increased line-width from 745 nm to 1.2 µm due to the exceeded buckling threshold of the PDMS stamp. A higher RMS value of 47±0.3 nm was estimated for the replica compared with that of 41±0.4 for the stamp.

In the case of the TGZ 2 stamp, features with roof collapse, decrease in the height by about 30 nm, reduced periods from 2.9 µm to 1.9 µm, and increased width from 1.1 to 1.7 µm were imprinted. Poor replication fidelity of TGZ 2 stamp is also visible in the cross section of *Fig. 35b*. This rounding is partially due to an AFM tip artifact, but is mainly due to the resist being forced to fill the mold recess. In addition, the measured CA for CD and TGZ 2 imprints showed hydrophilic behavior.

3.3.3.1 Process repeatability and mold durability

A detailed reproducibility study using sPDMS stamps replica of CD and TGZ 2 master templates, mr-IT85 films and T-NIL technique was performed. Requirements addressed in 3.3.1.1 must be fulfilled in order to define the stamps used in this experiment as durable and reproducible. Please note that resist thickness was measured in the middle region for only two coated substrates. Therefore, in a set of ten coated substrates, we will assume variable resist thickness ranging from 85 nm to 120 nm. Imprint temperature was 140°C for 2 min as recommended by the manufacturer's protocol.

The topography of the imprinted samples was examined by AFM. The pattern accuracy between the mold and the imprinted features was investigated using four metrics: height (h), period (p), width (w), and root mean square. AFM JPK software is used to accurately extract, the height, the periodicity and RMS values out of AFM scanning images. AFM cross section has been measured at three different random positions over the imprinted nanostructures. The average and standard deviation values of the three measurements are calculated and used to build the height, periodicity and RMS profiles.

A surface wetting experiment was carried out by water contact angle analyzer to measure the wettability of the imprinted surface. Contact angle values were obtained by averaging three measurements on different surface areas of the sample.

CD Stamp

First, mr-IT85 glass coated substrates were imprinted with sPDMS stamp replica of CD via T-NIL. The same stamp was used for all imprint cycles. The stamp was neither removed for cleaning nor for inspection purposes to avoid contamination. Given in *Fig. 36* is height profile with mean and standard deviation values vs. number of imprint cycles. The red line indicates the height of the stamp (118 nm).

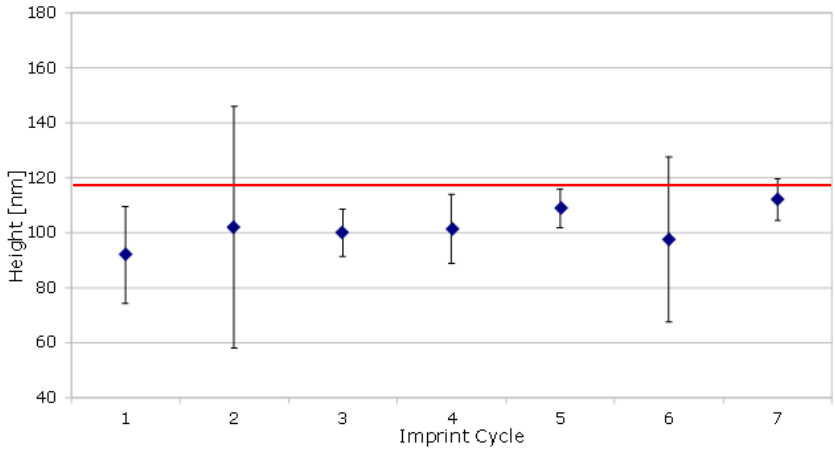

Fig. 36: Height profile of CD imprints with mean and standard deviation values.

Seven out of ten substrates were imprinted. The height profile in *Fig. 36* shows reduced heights compared with the stamp and an irregular height profile for all seven imprints. As a matter of variable resist thickness, irregularities in height were expected. *Fig. 37* illustrates the period length profile for seven mr-IT85 imprints. The red line implicates the estimated period length of the CD stamp.

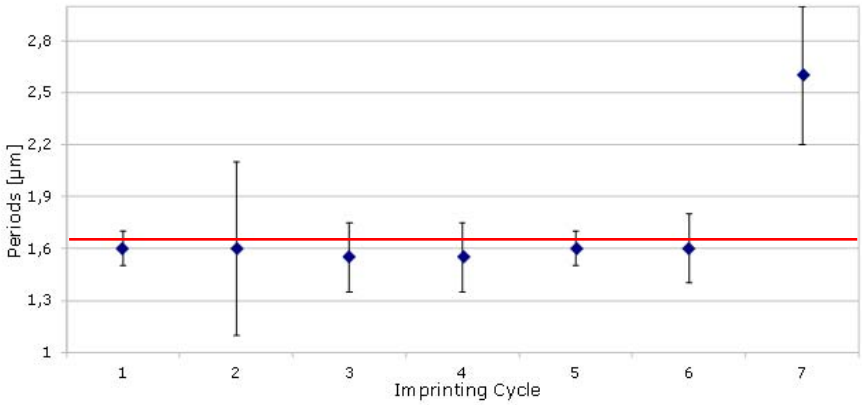

Fig. 37: Periodicity profile of CD imprints with mean and standard deviation values.

Period length during course of six imprint cycles was constant. However, high structural deformations and pairing were observed for the last imprint, also visible in *Fig. 38b*.

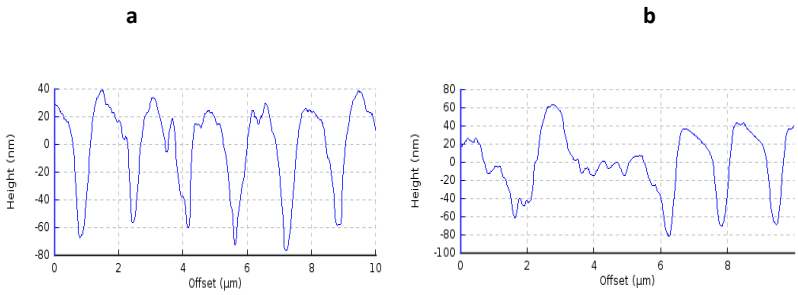

Fig. 38: AFM cross section images of CD imprints onto mr-IT85 film; (a) first imprint, and (b) last imprint.

The same structural deformations were reported previously in 3.3.1.1. Roof deformations in *Fig. 38a* were caused by the strong adhesion force between the resist and the mold during detachment. This implicates poor durability of the CD sPDMS stamp while imprinting mr-IT85 films.

TGZ 2 Stamp

Another set of EPON 1002F coated substrates was imprinted with TGZ 2 replica in sPDMS. The same stamp was used for all imprints. The pressure was applied on the top of the mold using tweezers to remove air bubbles, but was not kept constant during the imprint process. Given in *Fig. 39* is the height profile with mean and standard deviation values vs. number of imprint cycles. The red line indicates the height of the stamp i.e. 120 nm.

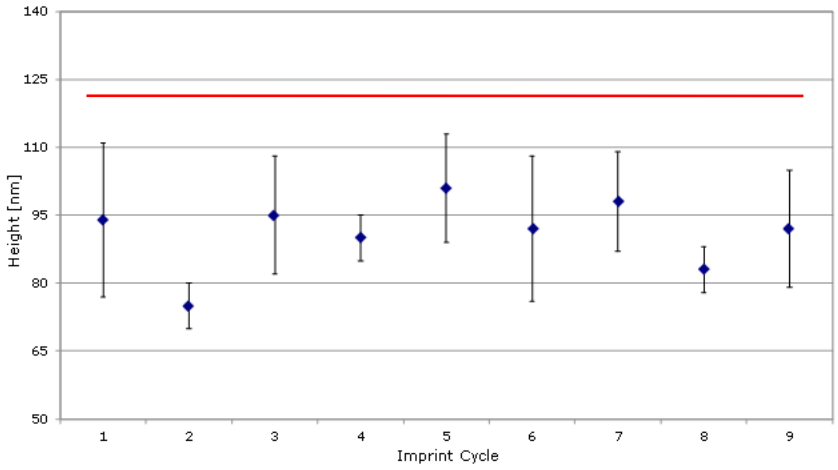

Fig. 39: Height profile of TGZ 2 imprints with mean and standard deviation values.

Nine out of ten substrates were imprinted. *Fig. 39* shows significant reduction in the height of the features compared to the mold height i.e. 120 nm. This can be attributed to the variable resist thickness. *Fig. 40* shows the period length profile for seven mr-IT85 imprints. The red line implicates the estimated period length of the TGZ 2 stamp.

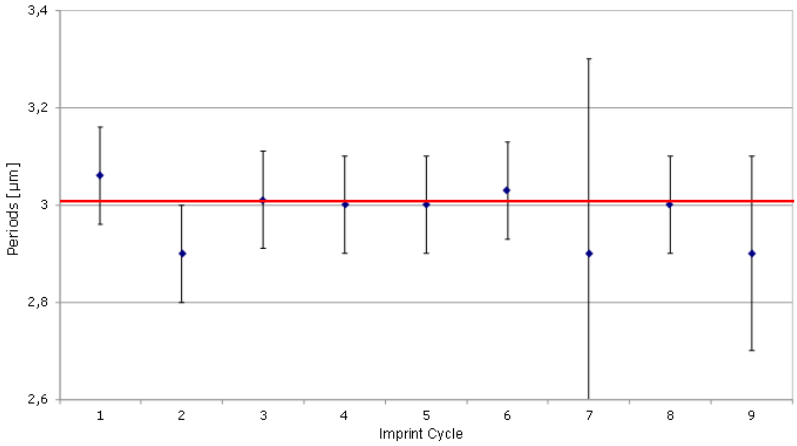

Fig. 40: Periods profile of TGZ 2 imprints with mean and standard deviation values.

Period length during course of nine imprint cycles was constant. However, non-uniformly distributed and distorted grating structures were obtained as shown in *Fig. 41 (a-b)*.

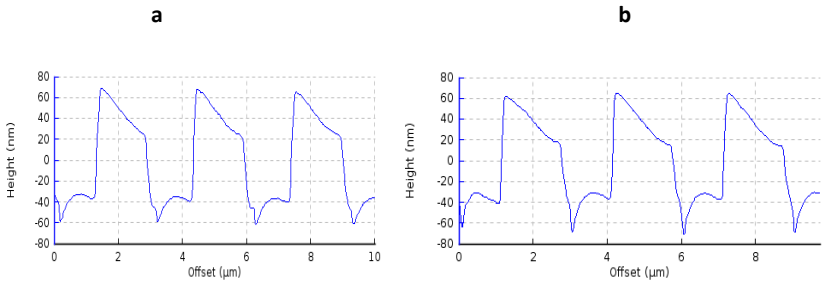

Fig. 41: AFM cross section images of TGZ 2: (a) first and (b) last imprint.

It is evident from *Fig. 41 a-b*, that the resist builds up in between the gratings. This implicates reflow of the resist. Most probably imprinting time must be longer to allow the resist to spread more uniformly around the gratings. However, the lateral size and the organization of the pattern were not affected. Nevertheless, our results implicate poor durability of the TGZ 2 sPDMS stamp while imprinting mr-IT85 films.

3.3.4 Summary

In this section, we employ T-NIL and imprinted EPON 1002F and mr-IT85 films with differently structured stamps. Further, accuracy of pattern transfer as well as reproducibility and durability of the stamps were investigated. Major differences are evident between the investigated resist and stamp materials.

In comparison, high quality and sub 75 nm patterns were successfully imprinted onto EPON 1002F films using Temicon sPDMS. The reproducibility of this stamp was also found to be excellent. Further, the best quality imprints with excellent reproducibility were obtained using TGZ 2 replica in sPDMS. On the other hand, structural deformations, low accuracy and limited reproducibility were observed in case of patterns imprinted with CD and TGZ 11 sPDMS and hybrid PDMS Mustapha stamps. However, those imprints are still good enough to be used for further experiments. Thus, our data implicate that Sylgard 184 PDMS is the best suitable stamp material for imprinting of EPON 1002F films via T-NIL.

On the other hand, using mr-IT85 resist, poor quality imprints were fabricated. The imprints performed by sPDMS replica mold of CD and TGZ 2 are characterized by high structural deformations and low transfer accuracy. In terms of reproducibility of the stamps, high variations in imprint profiles as well as high structural deformations of the features implicated poor reproducibility of CD and TGZ 2 sPDMS stamps. Therefore mr-IT85 was not investigated further as resist material in this thesis.

In addition, we believe that T-NIL using Ormostamps, as discussed in 3.2.3 is a promising method which however could not be realized as the imprinting machine was broken.

3.4. UV-NIL

In this section, we present results obtained with UV curable Amonil MMS 10, using two different stamp types of molds, e.g. sPDMS and hybrid PDMS. The transfer accuracy of the imprints as well as the reproducibility of the mold is reported. NIL printing was carried out in a lab environment at room temperature. The stamp was placed onto the substrate without applying any pressure and the mold/substrate configuration was exposed to UV light for 10 min by using a mercury lamp (200 watt). The topography of the texturized samples was examined by AFM. The pattern fidelity between the mold and the imprinted features is investigated using four metrics: height (h), period (p), width (w), and root mean square (RMS). AFM JPK software is used to accurately extract values out of AFM scanning images. AFM cross section has been measured randomly at three different positions over the imprinted nanostructures and average and standard deviation values were calculated. Estimated imprint profiles were further compared to corresponding stamp profile. In addition, the static water contact angle (CA) of the imprinted surface was measured.

3.4.1 Amonil Imprints using sPDMS stamps

Replica of four masters in sPDMS i.e. Temicon, CD, TGZ 2 and TGZ 11 were imprinted in Amonil MMS 10 films. Examples of various imprinted patterns are depicted in *Fig. 42 (a-d)*.

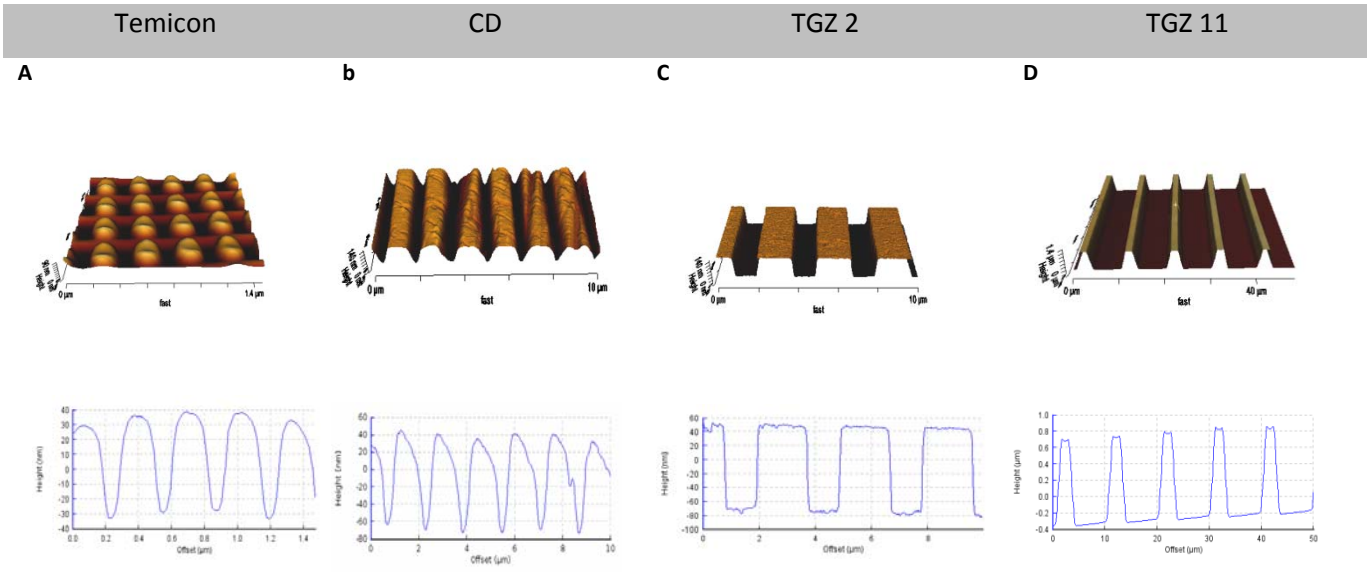

Fig. 42: AFM images of imprints onto Amonil MMS 10 films using (a) sPDMS Temicon, (b) CD, (c) TGZ 2 and (d) TGZ 11 molds.

Table 11 summarizes the values extracted from AFM cross section images for the Amonil MMS 10 imprints.

Table 11: Summary of mean and standard deviation values achieved for the Temicon imprint.

Replica	Height [nm]	Periods [nm]	Width [nm]	Deformations	Contact angle [Θ°)	RMS [nm]
Temicon	66±6.0	322±2.0	197±10	No	103±0.7	15±0.2

The stamp was brought in contact with the coated substrate and no pressure of any kind was applied. Please note that it was impossible to scan Temicon sPDMS stamp due to technical problems. Therefore, in order to access the accuracy of the imprinted patterns, the imprint profile was compared with the original master profile (Temicon master pad C2 has the height of 150±10 nm and the periodicity of 500±10 nm). An array of sub 70 nm pillars was faithfully replicated. The imprinted pillars have the height of about 66 nm, and periods of ~ 322 nm. Based on our data (*Table 11*), a reduction by 56 % in height of the imprinted pillars was observed. The transfer accuracy might be improved by applying pressure on the top of the stamp during the imprint process, thereby assuring better and conformal contact between the stamp and the substrate. Further, homogenous and excellent pattern structure (*Fig. 42a*) was observed. In addition, surface roughness is about 15 nm; the measured contact angle (103 °) indicates hydrophobic behavior of the imprint.

AFM scan and cross section image of the imprinted CD lines are depicted in *Fig. 42b*. The imprint was performed using 1.5 x 1 cm CD mold replica in sPDMS. *Table 12* summarizes the values extracted from AFM cross section image for used CD mold and the imprint.

Table 12: Summary of mean and standard deviation values as determined for the CD mold and imprint.

	Height [nm]	Periods [µm]	Width [nm]	Deformations	Contact angle [Θ°]	RMS [nm]
CD stamp	116±16	1,6±0.2	595±64	No	136 ±2.3	27±1.0
Imprint	101±13	1,6±0.2	800±18	No	107 ± 0.7	34±0.2

First, contact angle of the CD mold surface was measured before and after the imprint process. CA of 136° before imprinting indicated high hydrophobic properties of the stamp surface. CA after imprinting was 102°± 2 indicating decreased surface energy but still hydrophobic behavior. Further, the stamp was brought into contact with the coated substrate and no pressure of any kind was applied. The AFM cross section image *Fig. 42b* shows patterns with spiky rather than rounded roofs. The shape fidelity was governed by the shrinkage during polymerization. Overall, it can be seen from T*able 12*, that fine lines of reduced mean height by approximately 15 nm were imprinted. Further, constant period length of 1.6 µm and increased feature width by about 200 nm were measured. The surface roughness of the imprints is slightly enhanced to 34 nm compared to the stamp profile.

AFM images of imprinted TGZ 2 gratings are shown in *Fig. 42c*. Table 13 summarizes the values extracted from the AFM cross section image for the used TGZ 2 mold and the imprint.

Table 13: Summary of mean and standard deviation values obtained for the TGZ 2 mold and imprint.

	Height [nm]	Periods [µm]	Width [nm]	Deformations	Contact angle [Θ°]	RMS [nm]
TGZ 2 stamp	121±1.0	2,95	1112	No	108±2.3	56±0.5
Imprint	120±6.0	2,92	1.767±4	No	104 ± 2.6	27±0.5

The gratings with sharp, vertical and smooth edges similar to the original stamp with the mean height of 120 nm, and the period length of 2.9 µm were faithfully imprinted. A broadening by about 600 nm of the gratings was observed even though the general shape is maintained. Further, RMS was 27 nm. In addition, the contact angle of the imprinted surface was 104° implicating a more hydrophilic behavior compared with the non-structured surface.

AFM measurements were also carried out in order to better compare the surface of TGZ 11 imprint and TGZ 11 stamp. In *Table 14*, measured values for TGZ 11 sPDMS stamp and imprint are presented.

Table 14: Summary of mean and standard deviation values as determined for the TGZ 11 mold and imprint.

	Height [µm]	Periods [µm]	Width [µm]	Deformations	RMS [nm]
TGZ 11 stamp	1,37±0.2	10 ±0.4	7,2±1.8	No	558±5.0
Imprint	1,06	10±0.2	2,5±0.0	No	420±0.2

It can be seen from *Fig. 42d* that the fine grating structure was faithfully imprinted. The height is increased by 300 nm. On the contrary, the width is reduced by approximately 5 µm, whereas the periodicity remains unchanged. Additionally, the RMS is 420 nm.

3.4.2 Amonil-*h*PDMS Imprints

Hybrid stamp replica of Mustapha master as discussed in 3.2.2 was imprinted in a 100 nm thin Amonil MMS 10 film via the UV-NIL technique. The imprint was further investigated by AFM operated in contact mode. AFM scans were further analyzed with regard to features height (h), period (p), width (w) and root mean square (RMS). The average and standard deviation values of height, periods, width, RMS and CA summarized in *Table 16* were collected by measuring each imprint multiple times. Estimated imprint profiles were further compared to corresponding stamp profile. A surface wetting experiment was carried out to measure the wettability of the imprinted surface.

Contact angle values were obtained by averaging three measurements on different surface areas of the sample. Examples of Mustapha imprinted patterns are depicted in *Fig. 43*.

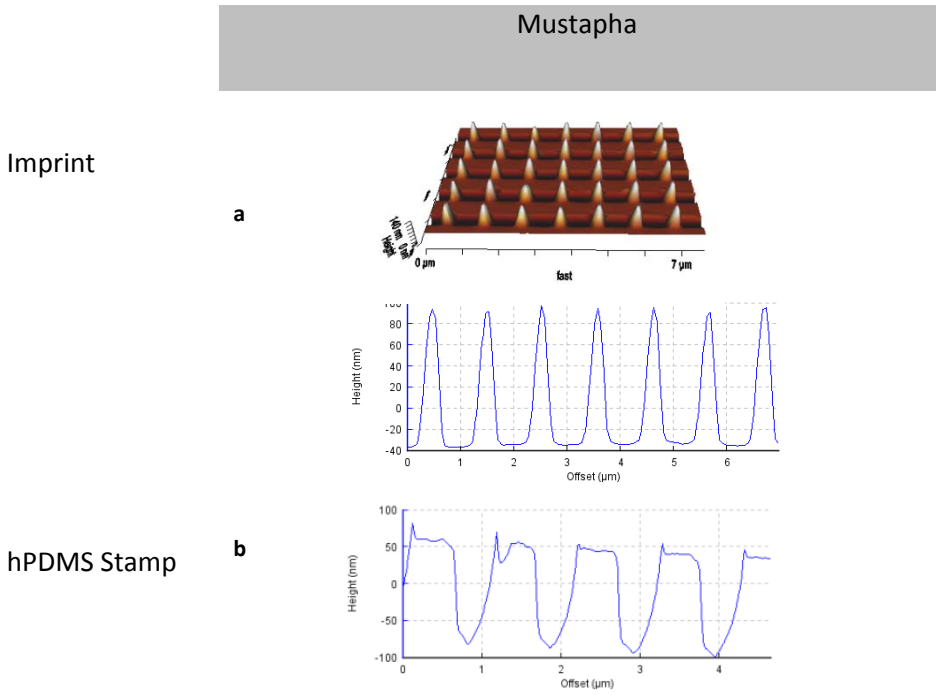

Fig. 43: AFM scan and cross section images of Mustafa imprint onto (a) Amonil film in comparison with (b) hPDMS stamp.

Table 15 summarizes average and standard deviation values extracted from AFM cross section images for fabricated Mustapha hybrid stamp.

Table 15: Summary of mean and standard deviation values determined for Mustapha hybrid PDMS mold and imprint.

Imprint	Height [nm]	Periods [µm]	Width [nm]	RMS [nm]
Mustapha stamp	130±11	1	688±35	54±3.0
Imprint	129±4.0	1	282±3.0	46±1.0

AFM measurements revealed uniformly distributed pillar structures. The average height is reduced by 2 nm respectively, the period length is 1 µm and the width is decreased by approximately 400 nm. The decreased RMS from 54±3 nm to 46±1 nm implicates a smoother sidewall surface of the imprinted pillars. The quality and uniformity are excellent and in good agreement with the mold.

3.4.3 Reproducibility and sPDMS mold durability

Durability and reproducibility of sPDMS stamps replica of CD, TGZ 2, TGZ 11 and Temicon masters, imprinted onto Amonil MMS 10 films via UV-NIL were studied. The topography of the imprinted samples was examined by AFM. Contact angles of the imprinted surfaces were measured to estimate surface wettability. The values were obtained by averaging three measurements on different surface areas of the sample.

CD stamp

First, Amonil MMS 10 glass coated substrates were imprinted with sPDMS stamp replica of CD via UV-NIL technique. The same stamp was used for all imprint cycles. The stamp was neither removed for cleaning nor for inspection purposes to avoid contamination. Given *in Fig. 44* are the AFM cross section images for the first and last Amonil MMS 10 imprints.

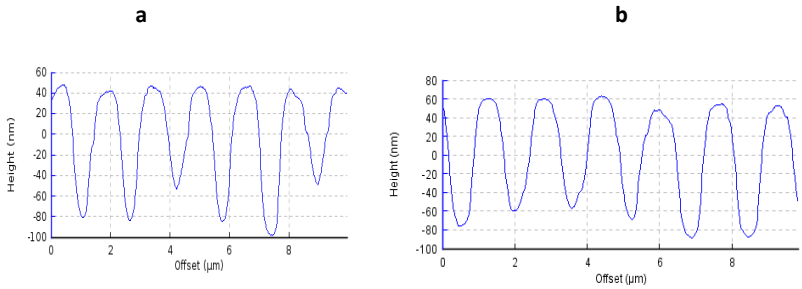

Fig. 44: AFM cross section images of CD imprints onto Amonil films for the (a) first and (b) last imprint.

All ten substrates were successfully imprinted. The grating structures are uniformly distributed and no structural degradation was observed. Given in *Fig. 45* is the height profile with mean and standard deviation values vs. number of imprint cycles. The red line indicates the mean height of the stamp (127 nm).

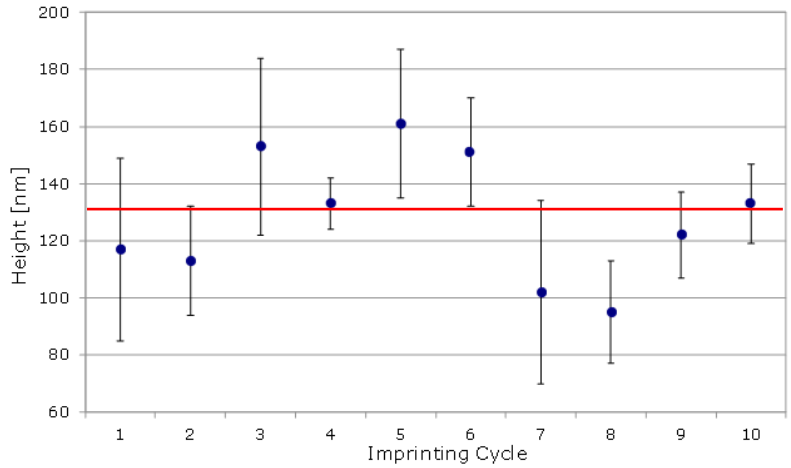

Fig. 45: Height profile of CD imprints with mean and standard deviation values.

As can be seen in *Fig. 45* the average height of the imprinted features sharply increases after the second imprint from ~117nm to 155 nm followed by a sharp decline in imprint height and subsequent increase after another eight imprints. The periodicity profile in *Fig. 46* shows minor variations compared to the stamp. The red line indicates the periodicity of the stamp.

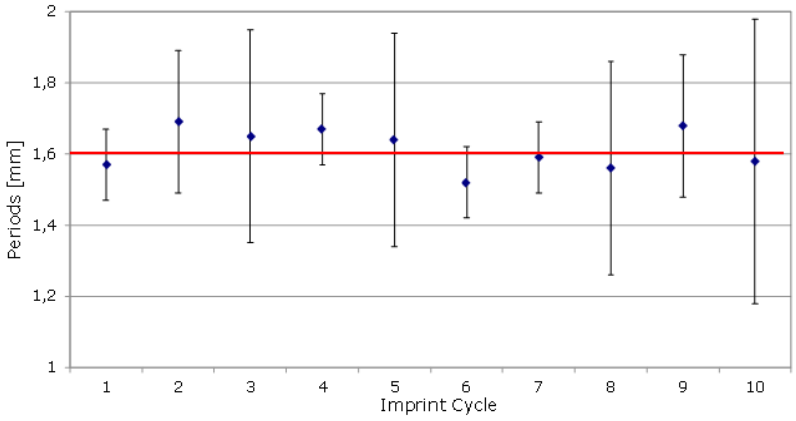

Fig. 46: Periodicity profile of CD imprints with mean and standard deviation values.

The fidelity of periodicity between the line features turned out to vary between 1.5 and 1.7 µm. Further, RMS values were estimated and depicted in *Fig. 47*. The RMS of the stamp is 27 nm.

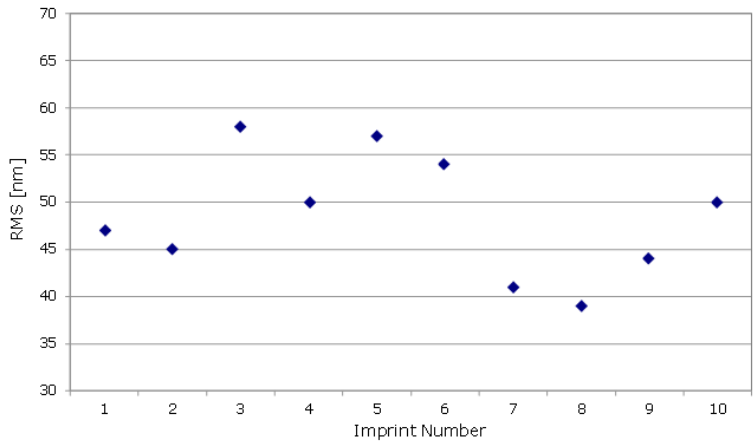

Fig.47: Surface roughness profile of CD imprints with mean values.

RMS is increased compared with the stamp profile. This implicates a rougher surface of the imprinted substrates. Moreover, surface roughness correlated well with the height of the patterned lines. Data point distribution of RMS (*Fig. 47*) and estimated height (*Fig. 45*) have identical pattern. As the roughness of the features decrease, the height tends to decrease as well and inversely, implicating non-accurate imprinting. In addition, Fig. 48 illustrates average CA values obtained for five substrates, patterned with CD working stamp and five un-patterned resists exposed to UV light.

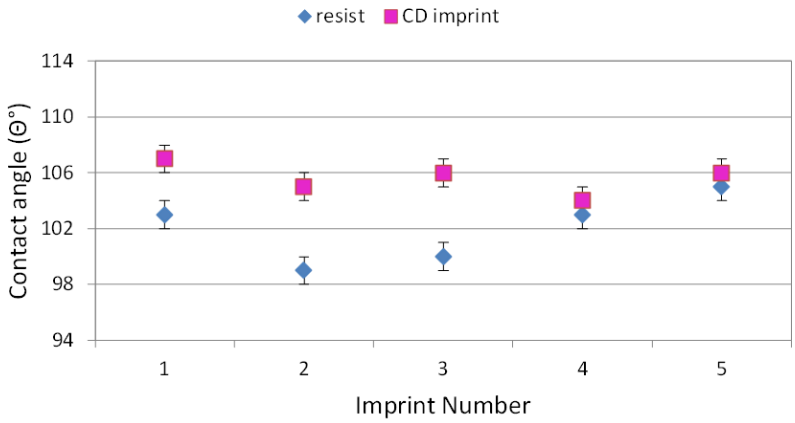

Fig. 48: Wettability profile of five CD imprints with mean and standard deviation values.

CA of unexposed Amonil MMS 10 was 86° ± 0.3°. As one can see in *Fig. 48*, the CA of spin coated resist exposed to UV light varies between 103° and 105° and the CA of nanostructured substrates further slightly increases to 107° during five imprint circles.

Nevertheless, these data do not establish a clear link between surface roughness and wettability of the imprinted surface.

TGZ 2 stamp

Another set of Amonil MMS 10 coated glass substrates was imprinted with TGZ 2 replica in sPDMS. The AFM cross section images shown in *Fig. 49* compare the structural quality of the first and the last imprint.

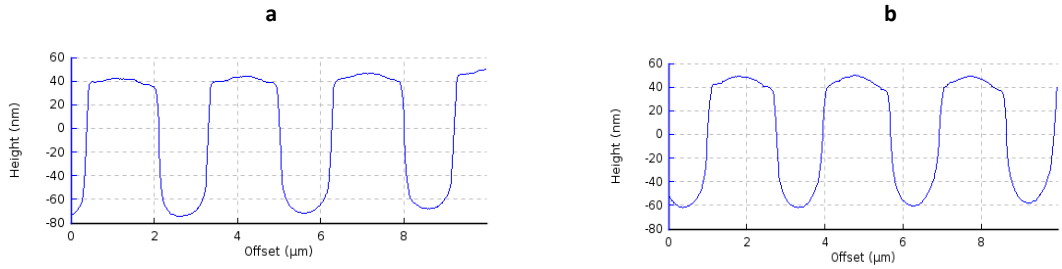

Fig.49: AFM cross section images of TGZ imprints onto Amonil films of the (a) first and (b) last imprint.

Nine out of ten substrates were imprinted. The most reliable imprints were obtained for the first six imprints. In *Fig 49a*, we see grating structures with flat roof shape, and straight sidewalls. Regardless, good gratings shape, the spacing between the features is rounded, rather than flat (*Fig.49b*). Subsequently, somewhat rounded edge geometry of the imprinted features was observed in *Fig. 49b* after the sixth imprinting cycle. As a consequence, minor reduction in periodicity was registered as shown in *Fig. 50*, which plots the periodicity against the number of imprints during nine imprinting cycles. The red line implicates the period length of the TGZ 2 stamp.

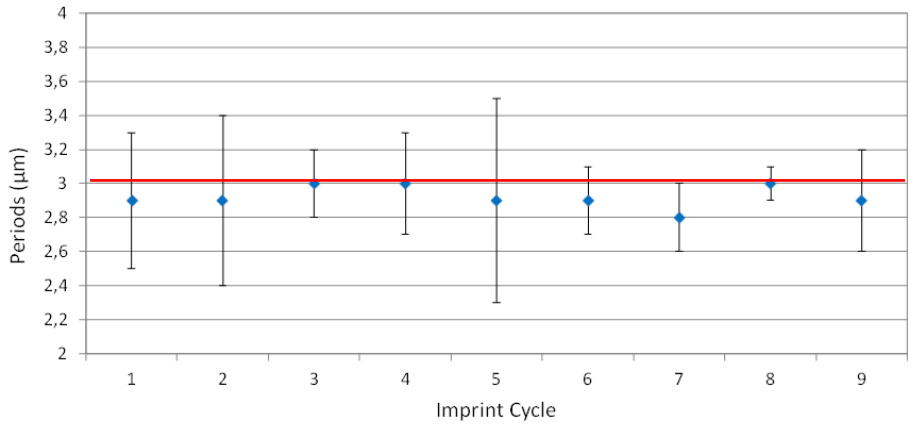

Fig.50: Periodicity profile for TGZ 2 imprints with mean period length values.

The periodicity is quite constant, matching the stamp profile. Moreover, the height is reduced as illustrated in *Fig 51*. The red line implicates the estimated height of the TGZ 2 stamp (121 nm).

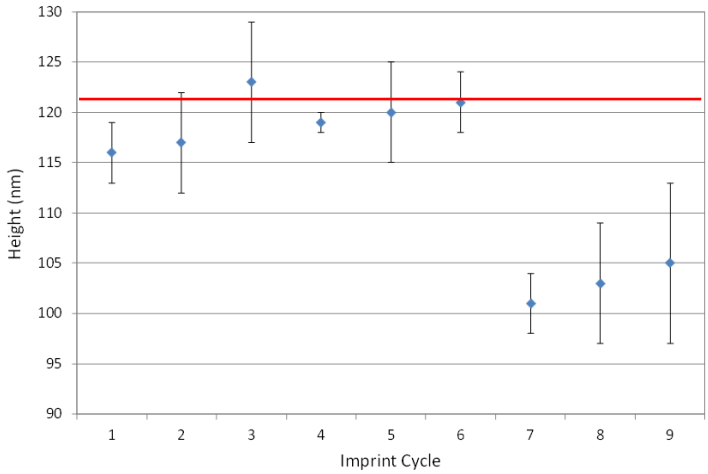

Fig. 51: Height profile for TGZ 2 imprints with mean and standard deviation values.

The mean height for the first six imprints is between 116 and 121 nm, matching well the stamp height. With further imprints, the height drops to 101 nm. *Fig. 52* shows the RMS profile for the nine imprinted substrates. RMS of the stamp is 56 nm.

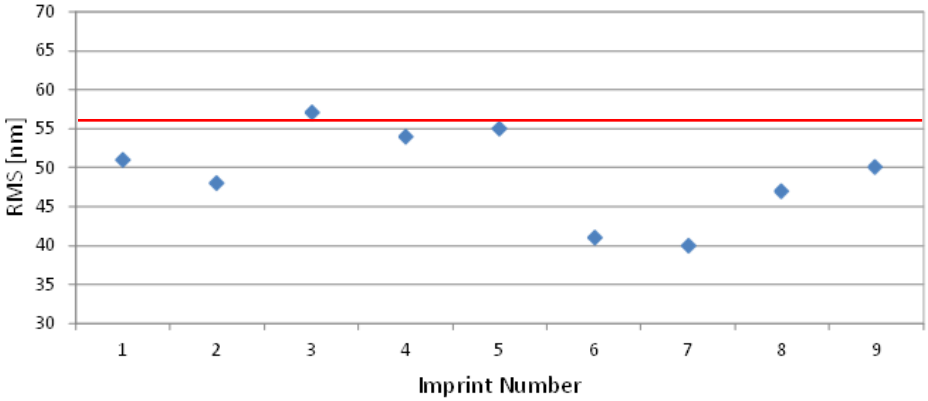

Fig. 52: Surface roughness profile for nine TGZ 2 imprints with mean values.

There was no significant difference in surface roughness between our stamps and imprints. The first 5 imprints had a mean roughness of a few nm following the surface roughness of our initial stamp. After 5 imprints, high decrease of the imprinted grating roughness is observed, meaning that significant degradation of our working stamp appears at this stage.

In addition, direct correlation between RMS and imprint height was observed. Data point distribution of RMS (*Fig. 52*) and estimated height profile (*Fig. 51*) have identical pattern. The reduced surface roughness reflected in the height reduction, confirms non-accurate imprinting and stamp degradation. Given in *Fig. 53* are measurements obtained for five TGZ 2 imprints and resist films exposed to UV light during imprinting. Please note that the CA of the plain resist films after spin coating was 96.1 ± 0.5.

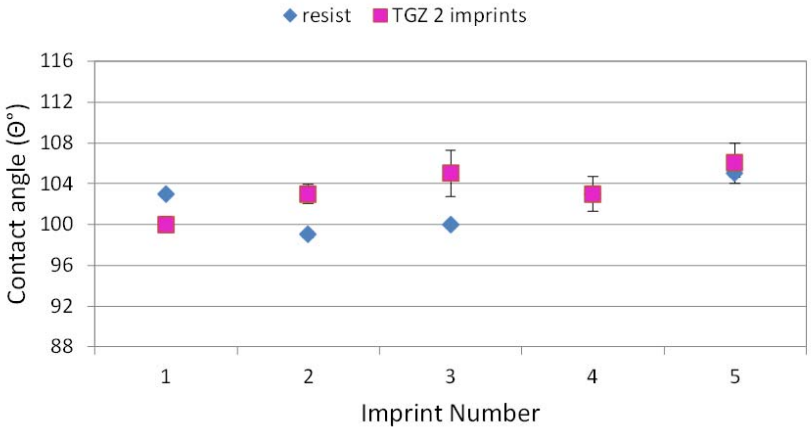

Fig. 53: Wettability profile of five TGZ imprints with mean and standard deviation values.

Exposure of the resist to UV light results in increased CA. The CAs of the imprints suggests a hydrophobic surface. Moreover, surface wettability increases with increasing surface roughness as deduced from *Fig. 52 and Fig. 53*.

Temicon stamp

Next, durability of Temicon replica in sPDMS during UV-NIL was investigated. The same conditions apply as decribed previously. The AFM cross section images shown in *Fig. 54* compare the structural quality of the first and the last imprint. Please note that only one pad per imprint is scanned, randomly.

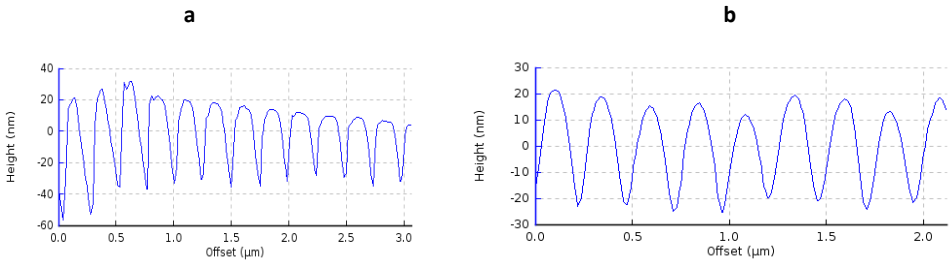

Fig. 54: AFM cross section images for the (a) first, and (b) last Temicon imprint.

Ten out of ten substrates were successfully imprinted. The cross section image in *Fig. 54a* illustrates high quality imprinted pillars with a mean height of ~42 nm and a mean periodicity of ~250 nm. Low values of the average RMS (19 nm) indicate a very smooth surface of the imprint. *Fig. 29 b* shows pillars with an average height of ~36 nm, average spacing of 260 nm and RMS of 16 nm. Finally, high quality imprints, free of any structural degradation prove excellent durability and repeatability of the Temicon sPDMS stamp.

3.4.3 Summary

In this section, we showed that sPDMS and hybrid PDMS are suitable materials for successful replication of high quality line-, grating- and pillar patterns in Amonil MMS 10 coated substrates by UV-NIL. Additionally, reproducibility and durability of the mold was studied. In comparison, using sPDMS, the highest durability as well as accuracy was observed in nanoimprinting of TGZ 2 and Temicon features. On the other hand, Mustapha hybrid PDMS stamps could be used for one imprint only.

3.5 AUTOFLUORESCENCE

Only substrates with low autofluorescence at the excitation wavelength are suitable for application in protein arrays. Thus, the optical properties of EPON 1002F and Amonil MMS 10 patterned surfaces were investigated. In a protein array experiment, we then studied the binding capacity of the un-patterned and patterned surfaces. To do so, we assessed the autofluorescence and assay performance of the resist after spin coating and the resist treated with temperature or UV light. Further, to corroborate the hypothesis that a patterned surface provides enhanced protein binding as a result of increased surface area a flat PDMS stamp pressed onto the resist and different imprints, namely fabricated from Temicon, Mustapha, CD, TGZ2 and TGZ 11 molds were investigated. To compare the autofluorescence of the substrates, all samples were scanned at a photomultiplier tube (PMT) setting of gain 1000 Volt for red (635 nm) and green (523 nm) light using a GenePix 4000B array scanner. Autofluorescence was quantified with GenePix Pro 6.0 software. Mean values and SDs of all replicates were calculated.

3.5.1. EPON 1002F

An optical investigation of EPON 1002F imprinted substrates was first carried out. *Fig. 55* illustrates the autofluorescence of EPON 1002F imprints together with three reference surface i.e. (i) resist after spin coating, (ii) resist exposed to 95°C for 1 min i.g. resist t° and (iii) flat PDMS pressed onto the resist. The Temicon, Mustapha, CD, TGZ 2 and TGZ 11 bars are arranged in ascending order of their pattern densities i.e. from 350 nm to 10 µm.

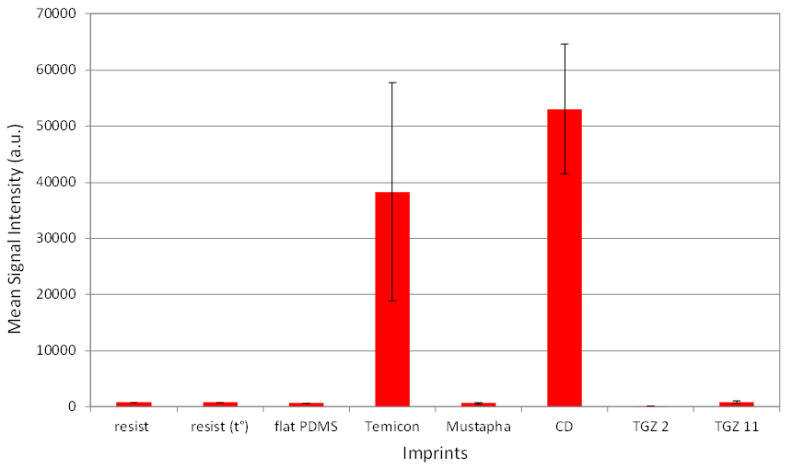

Fig. 55: Red light autofluorescence signal of the EPON 1002F imprints with references, scanned at PMT 1000 V.

As obvious from *Fig. 55,* CD line-patterned chips show the highest autofluorescence at λ_{ex}=635 nm followed by Temicon pillar structured surface. While the Temicon and CD nanostructured chips display a saturation of relative signal intensities, other chips such as Mustapha, TGZ 2 and TGZ 11 exhibited a 20 to 30-folds lower degree of red autofluorescence. This phenomenon is also evident in *Fig. 56* which illustrates autofluorescence values under green light excitation (λ_{ex}=532 nm).

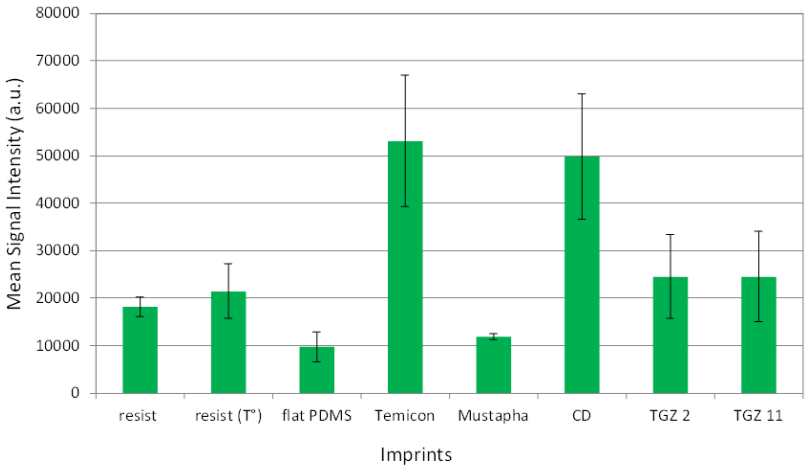

Fig. 56: Green light autofluorescence of the EPON 1002F imprints with references, scanned at PMT 1000 V.

In general, autofluorescence at green light excitation was increased compared with red light excitation. The Temicon pillar-patterned chips show the highest autofluorescence followed by the CD line-patterned surface. The lowest autofluorescence was obtained for flat PDMS (unstructured surface).

Our results suggest that the autofluorescence signal intensity correlates with the variable height of the imprinted features. Temicon and CD imprints are characterized with variable features across the imprinted surface, in case of Temicon heights are ranging from 4 to 25 nm and in case of CD imprints heights are from 40 to 120 nm. On the contrary, Mustapha, TGZ 2 and TGZ 11 imprints have a homogenous height profile over the whole imprint area.

3.5.2. Amonil MMS 10

Furthermore, the autofluorescence of Amonil MMS 10 imprinted substrates was scanned. *Fig. 57* illustrates the autofluorescence signal of the Amonil MMS 10 imprints together with two reference values: (i) resist exposed to UV light for 2 min i.g resist UV and (ii) a flat PDMS onto coated glass substrate under red light excitation (λ_{ex}=635). Flat PDMS stamp, Mustafa, CD, and TGZ 11 bars are arranged in ascending order of their pattern densities e.g. from 1 µm nm to 10 µm.

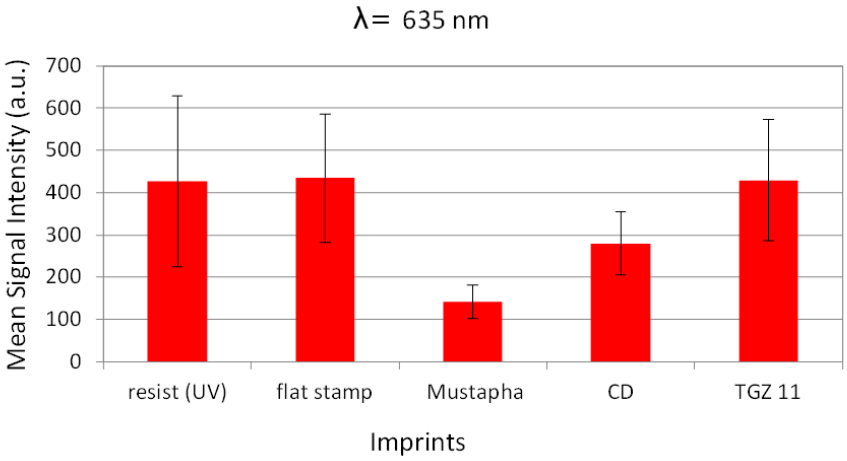

Fig. 57: Red light autofluorescence of the Amonil MMs 10 imprints with references, scanned at PMT 1000 V.

The same pattern but higher autofluorescence intensity was observed for green light excitation illustrated in *Fig. 58*.

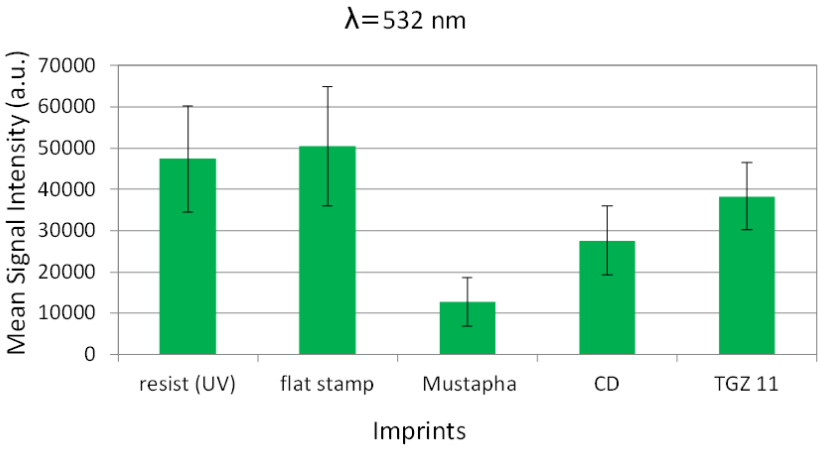

Fig. 58: Green light autofluorescence of the Amonil MMS 10 imprints with references, scanned at PMT 1000 V.

Under red-green excitation, we see that the reference surfaces have a higher signal intensity compared with the autofluorescence of the imprinted surfaces. There are several possible explanations:

Firstly, for un-patterned substrates the background noise comes from surface scattering. Secondly, during the imprinting process, the thickness of the resist decreases and as a consequence the autofluorescence is diminished. Further, it can be seen that the height and periodicity of the features reduce the background noise. The lowest background noise in both cases i.e. red-green light revealed the surface imprinted with Mustapha hybrid PDMS stamp with the height of 129 nm and periodicity of 1 µm. On the other hand, the surface imprinted with TGZ 11 sPDMS stamp with the height of 1 µm and the periodicity of 10 µm shows two times higher autofluorescence. Accordingly, our findings suggest that increase in the surface height and periodicity lead to a higher autofluorescence signal.

3.6. ASSAY PERFORMANCE

Chip processing is described in 2.1 followed by fluorescence detection introduced in 2.11.

3.6.1 EPON 1002F Assay

To recapitulate, following nanostructured substrates were fabricated via T-NIL for protein immobilization: (i) Mustapha, an array of pillars of 70 nm height 1 µm period, (ii) TGZ 2, a grating with 120 nm height and 3 µm periodicity, (iii) TGZ 11, a grating with 2 µm height and 10 µm periodicity, (iv) CD, lines of 110 nm height and 1.6 µm spacing, and (v) Temicon, an array of discs. All substrates were scanned at PMT 1000V/1000V. The median values for EPON 1002F assay with 200 ng/mL Dy647- und Dy547-labeled anti CRP, after subtracting autofluorescene (see 3.5.1) for red light excitation are shown in *Fig. 59*.

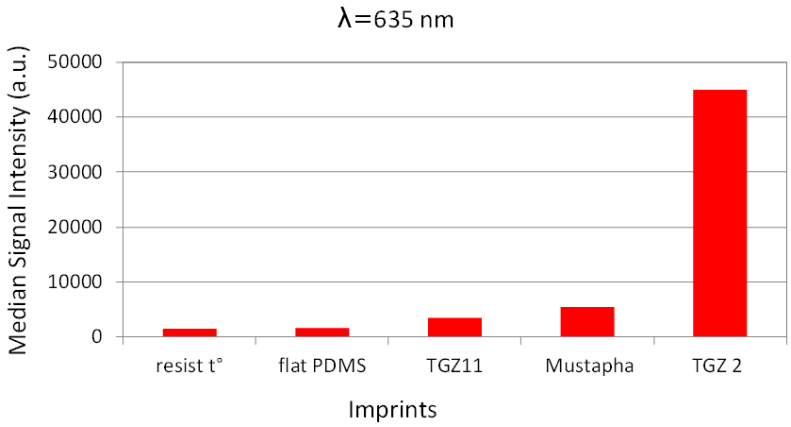

Fig. 59: Median intensity values for a CRP assay on EPON 1002F under red light excitation.

The overall assay performance was analyzed by comparing fluorescence signals on imprints and on control substrates e.g. resist t°, representing protein binding on the resist after exposure to temperature and flat PDMS, representing protein binding to the plain, unstructured surface. The protein binding on Temicon and CD patterned substrates could not be analyzed due to high autofluorescence. On imprints of TGZ 11 and Mustapha, signal intensities are slightly increased compared to control values, but still remain under 10000 a.u. The highest signal intensity was observed on imprints with TGZ 2. The TGZ 2 signal is increased by about 5 fold compared to other imprints. To commemorate, TGZ 2 and Mustapha substrates have smaller aspect ratio compared to TGZ 11.

Further, *Fig. 60* Illustrates median values for EPON 1002F assay with 200 ng/mL Dy647 und Dy547 anti CRP, with deducted autofluorescence for the green light excitation.

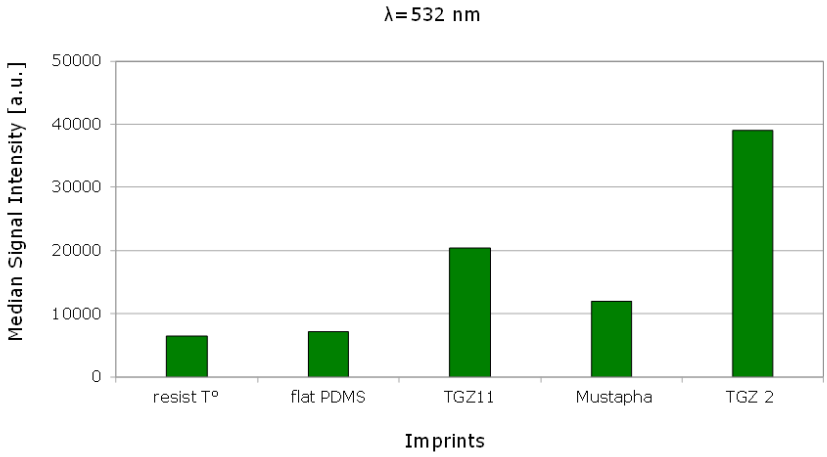

Fig. 60: Median intensity values for the EPON 1002F assay under green light excitation.

The resist t° and flat PDMS show lower signal intensities then under red light excitation. Further, TGZ 11 and Mustapha are increased by about 2 fold compared to the red light excitation profile. In addition, TGZ 2 shows the highest signal intensity compared to other imprints, and about 3 fold higher as assessed for the resist and un-patterned EPON 1002F surface.

3.6.2 Amonil MMS 10 Assay Performance

Amonil MMS 10 is an organic/ inorganic UV curable photoresist. As such, this material does not possess epoxy functions required for covalent binding of proteins to the solid surface. Hence, in order to immobilize proteins on the surface of Amonil MMS 10 patterned glass substrates (see 3.4), the chips were pretreated with a 3- glycidoxypropyltriethoxysilane (GOPS), a silica-surface modifier. The silanization procedure resulted in a substrate surface functionalization with epoxy rings. Prior to assay processing, CD, TGZ 2, Temicon, chips were immersed in 1% GOPS solution in a ratio 95/5 methanol/water at room temperature, covered with aluminum foil and placed on a lab shaker for 5, 10, 15, 30 and 60 min. Afterwards, the chips were washed 2 times with ethanol, blown dry with nitrogen, and investigated by AFM. The AFM inspection of the chips pretreated with GOPS for 5 and 10

min showedintact imprinted patterns. On the other hand, 15 min modification with GOPS led to high structural deformations of the imprinted patterns, while 30 and 60 min modification led to a complete disappearance of the imprinted structures.

Further, chips modified with GOPS for 10 min were processed as described in 2.10. *Fig. 61* illustrates a fluorescence scan of a surface of imprinted with Temicon, TGZ 2 and CD.

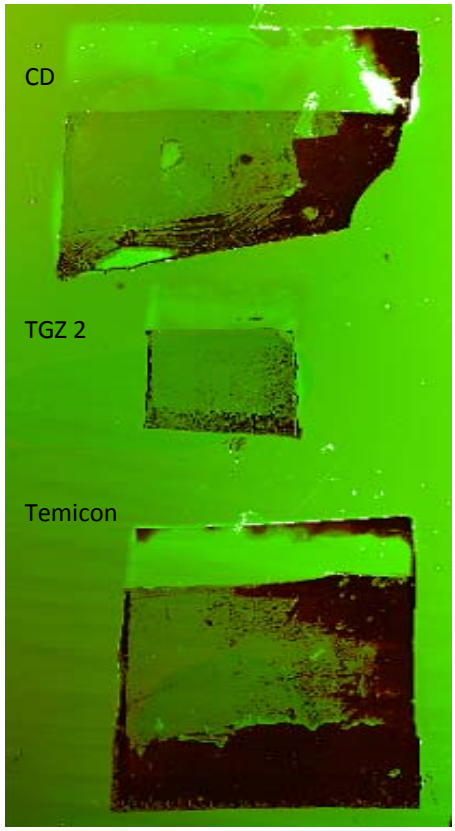

Fig.61: Amonil MMs 10 chips after protein immobilization.

The substrates feature a high level of autofluorescence and probably no protein binding occurred. We assume that GOPS treatment was insufficient to bind proteins onto Amonil MMS 10 nanostructured surfaces. Since we are not aware of the chemical composition of the Amonil resist, from this point of view it is impossible to further investigate these findings.

Conclusion

The results of this work confirm that nanostructuring based on nanoimprint lithography under mild conditions, such as room temperature and low pressure can be useful for protein array applications. Difference between T-NIL and UV-NIL is distinct. Both techniques allowed replication of high quality patterns into resists layers. However, improvement, especially concerning spin coating of uniform films, stamp durability, repeatability and defect control, is necessary to fabricate high quality nanostructured surfaces with good reproducibility to be implemented in protein arrays for improved assay performance.

Moreover, we showed that nanostructured epoxy surfaces effectively impact protein immobilization and signal enhancement. A signal enhancement of up to a factor of 30 in comparison to bare unmodified surfaces was reported. On the contrary, nanostructured Amonil MMS 10 surfaces are not appropriate for protein array applications as they are not capable of binding proteins.

We further demonstrated that a high throughput nanostructured platform for protein immobilization requires regular nanostructure dimensions over the entire patterned surface area in order to minimize background interference of the photoresist materials. In the future, sensitivity of the protein array chips could be further improved by using epoxy based materials, with low background interference, patterned with high resolution features. More experiments on ultrathin uniform layers and nano-imprinting of high resolution structures (< 50 nm) as well as a better understanding of the optical properties of the photoresist materials and imprinted patterns may very well lead to more efficient use in protein arrays and generally, wider acceptance of this method in bio-applications.

References

[1] S.Hanash, Nature422, 6928 (2003).

[2]E. Phizick, P. Bastiaens, H. Zhu, M. Snyder, and S.Fields, Natur*e* 422, 6928 (2003).

[3] V. Espina, E. Woodhouse, J. Wulfkuhle, H. Asmussen, E. Petricoin, and L. Liotta, *J.* Immunol. Methods290, 1 (2004).

[4] B. Schweitzer, P.Predki, and M.Snyder, *Proteomics* (2003).

[5] I. Saaem, V. Papasotiropoulos, T. Wang, P. Soteropoulos, and M. Libera, J. Nanoscience and Nanotechnology Vol.7, 1–10, (2007).

[6] P. E. Scopelliti, G. Bongiorno and P. Milani, Combinatorial Chemistry & High Throughput Screening, 14, 206-2016 (2011).

[7] Qian Tang, San-Qiang Shi, Limin Zhou, J. of Nanoscience and Nanotechnology, Vol. 4, No. 8, (2004).

[8]Q. Tang, S.Shi, L. Zhou*,* American Scientific Publishers (*2006).*

[9]G.Y. Jung, S. Ganapathiappan, D.A.A. Ohlber, D. L. Olynick, Y. Chen, W. M. Tong, R. S. Williams, Nano Letters 4,7: 1225-1229 (2004).

10. S. Y. Chou, P. R. Krauss, and P. J. Renstrom, Appl. Phys. Lett. 67,3114 (1995).

[11]http://www.streetdirectory.com/travel_guide/14714/gadgets/latest_semiconductor_lithography_developments.html

[12]S. Y. Chou, P. R. Krauss, and P. J. Renstrom, J. Vac. Sci. Technol. B 14(6), (1996).

[13] J. Viheriälä, T. Niemi, J. Kontio and M. Pessa, Nanoimprint Lithography - Next Generation Nanopatterning Methods for Nanophotonics Fabrication, Recent Optical and Photonic Technologies, InTech (2010).

[14] M. Steward & C. Willson, MRS Bulletin, 30, 947-951 (2005).

[15] H.W. Ro, V. Popova, L. Chen, A.M. Forster, Y. Ding, K.J. Alvine, D.J. Krug, R.M. Laine, C.L. Soles, Adv. Mater. 10: 1-7 (2010).

[16] H. Lan and Y. Ding, Nanoimprint Lithography, Lithography, InTech (2010).

[17] T. Glinsner and G. Kreindl, Nanoimprint Lithography, Lithography, InTech (2010).

18. H. Schift and A. Kristensen,Handbook of Nanotechnology 3rd edition, Springer-Verlag, (2010).

[19]Xiaolin Wang, High Resolution 3D Nanoimprint Technology ; Template Fabrication, Kassel University Press (2011).

[20]P. Choi, F. Fu, L.J. Guo, Adv, Funct. Mater. 17: 65-70, (2007).

[21] H. Shift and A. Kristensen, B. Bhushan, Handbook of Nanotechnology 2nd edition, Springer-Verlag, (2007).

[22]T.T. Truonf, R. Lin, S. Jeon, H.H. Lee, J. Maria, A. Gaur, F. Hua, I. Meinel, J.A. Rogers, Langmuir , 23: 2898-2905 (2007).

[23] A. M. Armani, A. Srinivasan, and K. J. Vahala, Nano Letters,7(6): 1823(2007).

[24]J. N. Lee, C. Park, G. M. Whitesides, Anal. Chem.,75: 6544 (2003).

[25] A. Goyal, A.Kumar, P. K. Patra, S. Mahendra, S. Tabatabaei, P. J. J. Alvarez, G. John, P. M.

Ajayan, Macromol. Rapid Commun.,30: 1116–1122 (2009).

[26] K. M. Choi, J. A. Rogers, J. AM. Chem. Soc., 125, 4060- 4061 (2003).

[27]T.W. Odom, L.C. Love, D.B. Wolfe, K. E. Paul, G.M. Whitesides, Langmuir, 18: 5314 (2002).

[28] K. G. Sharp, G. S. Blackman, N. J. Glassmaker, A. Jagota, C.Y. Hui, Langmuir, 20, 6430-6438, (2004).

[29] H. Schmid, B. Michel, Macromolecules, vol. 33, issue 8, pp. 3042, (2000).

[30] T.Woo, O. Mitrofanov, J.W.P. Hsu, Adv. Funct.Mater., 15: 1683-1688 (2005).

[31] T.T. Truong, R. Lin, S. Jeon, H.H. Lee, J. Maria, A. Gaur, F. Hua, I. Meinel, J.A. Rogers, Langmuir, 23: 2898-2905 (2007).

[32]http://www.microresist.de/projects/transparent_nanostamp_evaluation_en.htm

[33] J. Perumal, Th. H. Yoon, H. S. Jang, J. J. Lee, D. P. Kim, Nanotechnology,20: 055704, (2009).

[34] M. Beck, M. Graczyk, I. Maximov, E.L. Sarwe, T.G.I. Ling, M.Keil, L. Montelius, Microelec. Engin. 61-62: 441-448 (2002).

[35] L. J. Guo, Adv. Mater. 19: 495-513, (2007).

[36] Y. Hirai, J. Photopolym. Sci. Technol., 18, 551, (2005).

[37]N.W. Kim, K.W. Kim, H. C. Sin, Micr. Eng. 86: 2324–2329, (2009).

[38] M. Dickey, M. Steward, G. Willson, Advanced Lithography, (2006).

[39] P. F. Fu, L. J. Guo and Xing Cheng, Material composition for nano- and micro-lithography, US Patent No: 7648767, (2010).

[40] http://www.lintec-usa.com/Contents/Products/Tape/Uvad.htm

[41] J. De Girolamo, M. Chouiki, J.-H. Tortai, C. Sourd, S. Derrough, M. Zelsmann, J.. Boussey, J. Vac. Sci. Technol. B 26: 2271, (2008).

[42] K. Wu, X. Wang, E. K. Kim et al., Langmuir 23(3), p. 1166-1170, (2007).

[43] E. P. Chan, and A. J. Crosby, J. Vac. Sci. Technol. B 24, p. 2716-2722, (2006).

[44] J.Boussey, Materials and anti-adhesive issues in UV-NIL, Dissertation (2010).

[45] X. Cheng, L. J. Guo, and P.-F.Fu,*Advanced Materials,* Vol. 17, pp. 1419-1424, (2005).

[46] E. K. Kim, N. A. Stacey, B. J. Smith, M. D. Dickey, S. C. Johnson, B. C. Trinque, and C. G. Willson, J. of Vacuum Science & Technology, Vol. 22, pp. 131-135, (2004).

[47]http://home.wanadoo.nl/tom.peeters/Subpaginas/spin%20coating.htm

[48] www.clean.cise.colubia.edu/process/spintheory

[49] www.microchemicals.eu/technical_information

[50]http://www.parkafm.com/AFM_technology/application_view2.php?id=193&cate=GeneralResearch

[51] J. H. Kim, H. J. Lee, K. Cho, S. Hur, J. Jeong, E. S. Lee, Korea Institute of Machinery and Materials, (2005).

[52] Wenjun Zheng, Surface Wetting Characteristics of Rubbed Polyimide Thin Films, Polymer

Thin Films, InTech (2010).

[53] P. Li, B. Lin, J. Gerstenmaier, and B.T. Cunningham, Vol. 99,6-13, (2004).

[54] http://www.imt.ro/echipamente/microarray_ploter.htm

[55] Shankaran, D. R., Gobi, K. V., Miura, N., Sens. Actuat., 121, 159-177 (2007).

[56] Oliver Poetz, Jochen M. Schwenk, Stefan Kramer, Dieter Stoll, Markus F. Templin, Thomas O. Joos, Mechanisms of Ageing and Development 126,161–170, (2005).

[57] http://www.imt.ro/echipamente/microarray_ploter.htm

[58] Biacore Concentration Analysis Handbook BR-1005-12 Edition AB.

[59] http://www.enzolifesciences.com/support/immunoassay-kits/immunoassay-basics/

[60] S. Ray, G. Mehta and S. Srivastava, Proteomics (2010).

[61] H. Zhu, M. Bilgin, M. Snyder, Proteonomic, 72:783-812 (2003).

[62] D.A. Hall, J. Ptacek, M. Snyder, Mech.Of Aging and Development, 128: 161-167, (2007).

[63] M. Sanchez- Carbayo, Proteins Microarrays, Springer Protocols, (2006).

[64] Dev Kambhampati; Protein Microarray Technology; WILEY-VCH Verlag, (2004).

[65] D. Fuard, T. Tzvetkova-Chevolleau, S. Decossas , P. Tracqui , P. Schiavone, Microelectronic Engineering vol. 85, 1289–1293, (2008).

[66] Microresist Technology, Berlin, Germany, http://www.rbchem.ru/includes/fckeditor/custom/File/microelectronics/Flyer_Ormocere_Mai_2009.pdf

[67] Harry j. Levinson, Lithography process control, Spie Press (1999).

[68] Nikhil D. Kalyankar, Novel Biosensors Using Intact Liposome Microarrays,Ph.D., City University of New York, (2007).

[69] Trimbach, D. et al.; Langmuir, vol. 19, 10957-10961, (2003).

[70] S. W. Lee and S. S. Lee, Microsystem Technologies 14, pp. 205-208, (2008).

[71] J. Escarre, K. Söderström, C. Battaglia, F. J. Haug, C. Ballif, Solar Energy Materials and Solar Cells, 881-886 (2011).

[72] J.S. Amin, E. Nikooee, Sh. Ayatollahi, A. Alamdari, Applied Surface Science 256, 6466-6472 (2010).

[73] A. Guo and X.Y. Zhu, CRC Press, Boca Raton, (2006).

Conference Presentations

Fabrication of Nanoimprinted Polymer Surfaces for Signal Enhancement of Protein Arrays in Medical Diagnostics- A. Salibasic, U. Sauer, C. Preininger; NanoBiomed 2012, Frankfurt, Germany- [Poster].

Protein Arrays using Nanoparticles and Nanostructures for improved Biomarker Diagnostics- C. Preininger, U. Sauer, J. Bawitsch, A. Salibasic, H. Herzog; 9th International Conference on Nanosciences & Nanotechnologies 2012, Thessaloniki, Greece – [Oral Presentation].

Nanoimprinted Polymer Surfaces for Signal Enhancement of Protein Biochips –U. Sauer, A. Salibasic, J. Bawitsch, C. Preininger; 38th International Micro & Nano Engineering Conference 2012, Touoluse, France – [Poster].